

Energetic footprints of irreversibility in the quantum regime

M. H. Mohammady,^{1,2,3,*} A. Auffèves,^{4,†} and J. Anders^{1,‡}

¹CEMPS, Physics and Astronomy, University of Exeter, EX4 4QL, United Kingdom.

²Department of Physics, Lancaster University, LA1 4YB, United Kingdom

³RCQI, Institute of Physics, Slovak Academy of Sciences, Dúbravská cesta 9, Bratislava 84511, Slovakia

⁴CNRS and Université Grenoble Alpes, Institut Néel, F-38042 Grenoble, France.

The unavoidable presence of irreversibility in classical thermodynamic processes carries two energetic footprints - the reduction of extractable work from the optimal, reversible case, and the generation of a surplus of heat that is irreversibly dissipated to the environment. Optimal thermodynamic protocols hence attempt to minimize irreversibility, quantified by the entropy production, subject to practical constraints. Recently it has been shown that in the quantum regime an additional quantum entropy production occurs, that can be linked to the fundamental irreversibility of a quantum system decohering into the energy basis. Here we employ quantum trajectories to construct distributions for classical heat and quantum heat exchanges, and show that the heat footprint of quantum irreversibility differs markedly from the classical case. We also quantify how the occurrence of quantum irreversibility reduces the amount of work that can be extracted from a state with coherences. Our results show that decoherence leads to both entropic and energetic footprints which play an important role in the optimization of controlled quantum operations at low temperature, including quantum processors.

I. Introduction

In recent years much effort has been made in extending the laws of thermodynamics to the quantum regime [1–4]. Maximal work extraction (or minimal work cost) has been discussed for a range of protocols [5–24], showing that energetic coherences can be a resource for work extraction [25–29] while quantum correlations can reduce the work cost of erasing information [30]. However, many of these studies have focussed on the optimal limit of reversible processes, i.e. unitary and quasi-static evolutions, without discussing the limitations that irreversibility puts on work extraction. On the other hand, the irreversibility of thermodynamic processes in the quantum regime has been explored using stochastic thermodynamics [31–39] leading to the notion of a fluctuating *quantum* entropy production [40] that obeys a fluctuation theorem analogous to those of classical non-equilibrium dynamics [41–43]. First experiments have now measured entropy production rates in driven mesoscopic quantum systems for two platforms, a micromechanical resonator and a Bose-Einstein condensate [44]. Most recently, the average entropy production of a quantum system that interacts with another (non-bath) system, has been shown to include an additional information flow term [45].

In classical thermodynamics irreversibility occurs whenever a non-thermal system is brought into contact with a thermal environment. The ensuing relaxation of the system leads to exchanges of energy that cannot be reversed with the same thermodynamic cost. In thermodynamics this irreversibility is quantified by the positive irreversible *entropy production* $S_{\text{irr}} := \Delta S - \frac{Q}{T} \geq 0$, which measures the discrepancy between the system's entropy increase $\Delta S = S_{\text{fin}} - S_{\text{ini}}$ during any thermodynamic process and

the heat Q absorbed by the system from the environment divided by the environment's temperature T . I.e. the heat fraction Q absorbed by the system in an irreversible process will be less than $T\Delta S$ giving a positive definite entropy production S_{irr} . Hence when a process has entropy production there is a surplus of heat,

$$Q_{\text{diss}}^{\text{sur}} = TS_{\text{irr}}, \quad (1)$$

that is irreversibly dissipated from the system to the environment [46]. Irreversibility also puts a fundamental bound on the amount of work W_{ext} that can be extracted during isothermal processes [46, 47],

$$W_{\text{ext}} = -\Delta F - TS_{\text{irr}} \leq -\Delta F, \quad (2)$$

where $\Delta F = F_{\text{fin}} - F_{\text{ini}}$ is the system's free energy increase. The more irreversible a process is, the less work can be extracted and the term $W_{\text{lost}} = TS_{\text{irr}}$ may be called the "lost" or non-recoverable work [48].

Eq. (1) and Eq. (2) link entropy production, S_{irr} to a surplus in heat dissipation, $Q_{\text{diss}}^{\text{sur}} \geq 0$, and a reduction in work extraction, $W_{\text{ext}} \leq -\Delta F$. These relationships are the well-known energetic footprints of irreversibility in classical thermodynamics. However, in the quantum regime, the link between entropy production and energetic footprints, such as the occurrence of a surplus of dissipated heat $Q_{\text{diss}}^{\text{sur}}$ and the lost work W_{lost} have remained elusive.

In this paper we establish the energetic footprints of irreversibility in the quantum regime, which arise whenever a system is brought in contact with a thermal environment. A quantum system can be out of equilibrium in two ways: by maintaining energetic probabilities that are non-thermal, and by maintaining coherences between energies. It has been shown that contact with the thermal environment gives rise to a classical and a quantum aspect of irreversibility [34, 35]. Here we go further and identify how each of the quantum and classical aspects of irreversibility leads to non-trivial energetic exchanges, i.e. we will discuss

* m.hamed.mohammady@savba.sk

† alexia.auffeves@neel.cnrs.fr

‡ janet@qipc.org

(classical) heat and work footprints, as well as the footprint of a uniquely quantum energy exchange known as quantum heat [23, 33, 36, 49–51].

For concreteness we here discuss a specific protocol that extracts work from a qubit's quantum coherences [27]. We extend the protocol here to capture irreversible steps that are unavoidable in any experimental implementation and which will affect heat and work exchanges. Employing quantum trajectories that describe the system's evolution during the entire protocol, we first show that the two entropy productions originate from the microscopic time-reversal asymmetry of quantum trajectories. Here we identify the distributions of classical and quantum heat, and evidence that purely quantum contributions to the entropy production are *not* related to the average quantum heat, in stark contrast to the classical regime, cf. Eq. (1). Instead, we show that the average quantum entropy production is correlated with the variance in quantum heat and, in the special case where the system is a qubit, both grow monotonically with the coherence in the quantum state with reference to the Hamiltonian, in contrast to the classical case. Finally, we show that the classical and quantum entropy production reduce the coherence-work in equal measure, cf. Eq. (2). The results show that when experimental imperfections are unavoidable, any work-optimization strategy needs to consider the trade-off between a system having a certain degree of classical non-thermality or quantum coherence, or both.

Besides being of fundamental importance for the development of a general quantum thermodynamics framework that includes irreversibility, these relations will also be crucial for the assessment of the energetic cost of quantum control protocols, that aim to optimize performance of computation and communication in the presence of decoherence and noise.

II. Imperfect protocol for work extraction from coherences

Readers familiar with work extraction from coherences [27] may skip the details of this section by looking at Fig. 1 and proceeding to Section III.

For a system with Hamiltonian H and quantum state ρ we denote by (ρ, H) any non-equilibrium configuration of the system, and by $(\tau, H)_T$ with $\tau := e^{-H/(k_B T)}/Z$ and partition function $Z := \text{tr}[e^{-H/(k_B T)}]$ its equilibrium configuration at temperature T [52]. For concreteness, we will here assume that the system is a qubit, but generalisations to larger dimensions are straightforward [27]. The qubit Hamiltonians throughout the protocol are chosen diagonal in the same basis, $H_j := \frac{1}{2} \hbar \omega_j (|e_+\rangle\langle e_+| - |e_-\rangle\langle e_-|)$ for $j = 0, 1, \dots, N$ with $|e_+\rangle$ the excited state and $|e_-\rangle$ the ground state and $E_{\pm}^{(j)} = \pm \hbar \omega_j / 2$ the energy eigenvalues. This means that only the spectrum of the Hamiltonian varies during the protocol.

The qubit's general initial state, written in its diagonal basis, is

$$\rho_\theta := p |\theta_-\rangle\langle\theta_-| + (1-p) |\theta_+\rangle\langle\theta_+|, \quad (3)$$

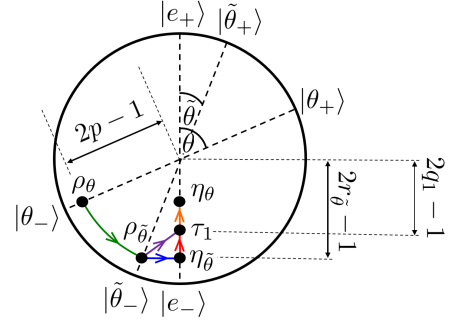


FIG. 1. **State evolution during work extraction protocol.** For the example of a qubit, in Step **(I)** the initial state ρ_θ is unitarily rotated (green arrow) to $\rho_{\tilde{\theta}}$, which may still have coherences with respect to the energy basis $|e_{\pm}\rangle$. The quench in Step **(II)** changes the splitting of the energetic levels but does not alter the state. The thermalization process (purple arrow) in Step **(III)** transforms the state $\rho_{\tilde{\theta}}$ to τ_1 , a thermal state diagonal in the energy basis $|e_{\pm}\rangle$. This process has a quantum component, i.e. decoherence (blue arrow) to state $\eta_{\tilde{\theta}}$ and a classical thermalization (red arrow) to state τ_1 . Step **(IV)** realises a (classical) quasistatic isothermal process (orange arrow) which transforms the state τ_1 to the protocol's final state η_θ . The quench in Step **(V)** leaves this state unaltered. This protocol realises the thermodynamic removal of coherences, i.e. transforming ρ_θ to η_θ , while irreversibility arises due to the mismatches between $\rho_{\tilde{\theta}}$ and $\eta_{\tilde{\theta}}$ as well as $\eta_{\tilde{\theta}}$ and τ_1 .

where $1 \geq p > \frac{1}{2}$ is the mixing probability and

$$|\theta_{\pm}\rangle := \cos(\theta/2)|e_{\pm}\rangle \pm \sin(\theta/2)|e_{\mp}\rangle, \quad (4)$$

are the two angle-dependent basis states of ρ_θ , see Fig. 1. The protocol transfers ρ_θ to the fixed final state η_θ chosen to have the same energetic probabilities as the initial state ρ_θ but with the energetic coherences removed [27]. I.e. $\eta_\theta := \sum_k \Pi[e_k] \rho_\theta \Pi[e_k]$ with $|e_k\rangle$ the energy eigenstates and $\Pi[\psi] = |\psi\rangle\langle\psi|$ denoting projectors onto pure states $|\psi\rangle$. Hence the qubit's final state is

$$\eta_\theta := r_\theta |e_-\rangle\langle e_-| + (1-r_\theta) |e_+\rangle\langle e_+|, \quad (5)$$

with $r_\theta := \langle e_- | \rho_\theta | e_- \rangle$ quantifying the projection of ρ_θ onto the ground state $|e_-\rangle$. We also define $q_j := \langle e_- | \tau_j | e_- \rangle$ as the ground state probabilities of the thermal states τ_j of the Hamiltonians H_j . Analogously to Eq. (3) and Eq. (5), states $\rho_{\tilde{\theta}}$ and $\eta_{\tilde{\theta}}$ can be defined for an angle $\tilde{\theta}$. Without loss of generality, we will limit θ and $\tilde{\theta}$ to fall in the range $[-\pi/2, \pi/2]$.

The optimal, reversible, implementation of the ρ_θ to η_θ transfer was proposed in [27] and it was shown that the “average” work extracted is $\langle W_{\text{ext}} \rangle = k_B T (S_{\text{vN}}(\eta_\theta) - S_{\text{vN}}(\rho_\theta)) \geq 0$, where S_{vN} is the Von Neumann entropy, defined as $S_{\text{vN}}(\rho) := -\text{tr}[\rho \log \rho]$. This is in agreement with equality in Eq. (2) assuming the free energy of a quantum non-equilibrium configuration is defined as $F(\rho, H) := \text{tr}[H \rho] - k_B T S_{\text{vN}}(\rho)$ [46, 47, 53–55], and realising that the state change ρ_θ to η_θ carries no energy change, $\Delta U = 0$, and hence $\Delta F = -k_B T \Delta S_{\text{vN}}$. We re-

mark that no distribution of work was provided in [27] with respect to which $\langle W_{\text{ext}} \rangle$ is an ‘‘average’’.

Generalizing first the steps of the optimal protocol [27] to include irreversibility will allow us to investigate the impact of entropy production on distributions of work and heat below.

The new protocol consists of the following five steps, and the state evolution is visualised for a qubit in Fig. 1:

- (I) Use a unitary V to rotate the quantum system’s configuration (ρ_θ, H_0) into configuration $(\rho_{\tilde{\theta}}, H_0)$. In the reversible protocol, V is chosen such that $\tilde{\theta} = 0$ and hence $[\rho_{\tilde{\theta}}, H_0] = 0$ [27]. Here we allow V to be imperfect and hence $\tilde{\theta} \neq 0$.
- (II) Change the Hamiltonian rapidly resulting in a quench from $(\rho_{\tilde{\theta}}, H_0)$ to $(\rho_{\tilde{\theta}}, H_1)$. In the reversible protocol, the energetic levels of H_1 are chosen such that the configuration $(\rho_{\tilde{\theta}}, H_1)$ is thermal at temperature T [27]. Here we consider the case that the energetic levels of H_1 are adjusted imperfectly, and hence configuration $(\rho_{\tilde{\theta}}, H_1)$ is not necessarily thermal.
- (III) Put the quantum system in thermal contact with a heat bath at temperature T . Assuming this step lasts longer than the system relaxation time, it brings the system from $(\rho_{\tilde{\theta}}, H_1)$ into the thermal configuration $(\tau_1, H_1)_T$.
- (IV) Change the system’s Hamiltonian slowly from H_1 to H_N , keeping the system in thermal contact with the heat bath. The evolution is chosen quasi-static (i.e. very slow), such that the thermal equilibrium at T is maintained throughout this step. The final Hamiltonian H_N is chosen so that the system’s thermal state is the desired final state, i.e., $\tau_N = \eta_\theta$.
- (V) Decouple the system from the thermal bath and quench the Hamiltonian back to H_0 , changing the system’s configuration from $(\eta_\theta, H_N)_T$ to the desired configuration (η_θ, H_0) .

Since steps (I), (II), (IV) and (V) are either unitary or quasi-static, they are reversible. The thermodynamic irreversibility of the protocol occurs when the quantum system is put in contact with the thermal bath in Step (III). The irreversible thermalization $(\rho_{\tilde{\theta}}, H_1) \rightarrow (\tau_1, H_1)_T$ leads to a reduction in free energy, i.e. $\Delta F^{(\text{III})} = -k_B T D[\rho_{\tilde{\theta}} \parallel \tau_1]$ where $D[\rho_{\tilde{\theta}} \parallel \tau_1] = \text{tr}[\rho_{\tilde{\theta}} (\log \rho_{\tilde{\theta}} - \log \tau_1)] \geq 0$ is the quantum relative entropy between the state before thermalization, $\rho_{\tilde{\theta}}$, and the state after thermalization, τ_1 , which vanishes if and only if $\rho_{\tilde{\theta}} = \tau_1$. Observing that no work is exchanged during thermalization ($W_{\text{ext}} = 0$), and based on the assumption that Eq. (2) holds in the quantum regime, the term $k_B D[\rho_{\tilde{\theta}} \parallel \tau_1]$ is often identified with the entropy $S_{\text{irr}}^{(\text{III})}$ that is produced during the thermalization step [35, 56].

As recently discussed in [34, 35], the geometric measure of irreversibility given by the relative entropy splits into a

quantum and a classical part,

$$D[\rho_{\tilde{\theta}} \parallel \tau_1] = D[\rho_{\tilde{\theta}} \parallel \eta_{\tilde{\theta}}] + D[\eta_{\tilde{\theta}} \parallel \tau_1], \quad (6)$$

which can be obtained as averages over the entropy produced along decoherence trajectories and classical thermalization trajectories [35], see also below. This splitting reflects the fact that the quantum configuration $(\rho_{\tilde{\theta}}, H_1)$ is out of equilibrium in two distinct ways: it can have non-Boltzmann probabilities for the energies and quantum coherences between energies. The coherence of $\rho_{\tilde{\theta}}$ with respect to the energy basis $|e_\pm\rangle$ of H_1 can be quantified by the overlap of $\rho_{\tilde{\theta}}$ ’s eigenstates, i.e.

$$\text{coh}(\rho_{\tilde{\theta}}) := 1 - |\langle e_+ | \tilde{\rho}_+ \rangle|^2 = \sin^2(\tilde{\theta}/2). \quad (7)$$

The classical non-thermality of $\rho_{\tilde{\theta}}$ compared to the thermal state τ_1 for H_1 can be quantified by the logarithm of the ratio of ground state probabilities [57], i.e.

$$\text{nonth}(\rho_{\tilde{\theta}}) := \log \frac{q_1}{r_{\tilde{\theta}}}, \quad (8)$$

where $q_1 := \langle e_- | \tau_1 | e_- \rangle$ and $r_{\tilde{\theta}} = \langle e_- | \rho_{\tilde{\theta}} | e_- \rangle = \langle e_- | \eta_{\tilde{\theta}} | e_- \rangle$ are the ground state populations of τ_1 and $\rho_{\tilde{\theta}}$, respectively, see Fig. 1. When both $\text{coh}(\rho_{\tilde{\theta}})$ and $\text{nonth}(\rho_{\tilde{\theta}})$ are zero then $\rho_{\tilde{\theta}}$ is an equilibrium state. Positive (negative) $\text{nonth}(\rho_{\tilde{\theta}})$ corresponds to a lower (higher) ground state population in $\rho_{\tilde{\theta}}$ than that of the thermal state τ_1 , corresponding to a down (up) red arrow in Fig. 1. The relaxation of a quantum state which is put in contact with a thermal bath naturally gives rise to two components of entropy production: a quantum contribution associated with the removal of coherences and a classical contribution associated with the classical thermalization of energetic state populations to become Boltzmann distributed. This splitting into decoherence (blue arrow) and classical thermalization (red arrow) is indicated in Fig. 1.

III. Stochastic quantum trajectories

Working on the level of density matrices of the qubit during the protocol, see Fig. 1, limits the discussion of thermodynamic quantities to macroscopic expectation values only. In contrast, stochastic thermodynamics associates heat $Q(\Gamma)$, work $W(\Gamma)$ and entropy production $s_{\text{irr}}(\Gamma)$ to individual microscopic trajectories Γ forming the set of possible system evolutions [58, 59]. In this more detailed picture the macroscopic thermodynamic quantities $\langle Q \rangle$, $\langle W \rangle$ and $\langle S \rangle$ arise as weighted averages over these trajectories. In the quantum regime, quantum stochastic thermodynamics captures the set of possible trajectories that, in addition to classical trajectories, are determined by quantum coherences and non-thermal sources of stochasticity [36, 38, 60–63]. These trajectories consist of time-sequences of pure quantum states taken by an open system in a single run of an experiment.

One way to experimentally ‘see’ quantum trajectories is by observing a sequence of stochastic outcomes of a generalized measurement performed on a system [64]. Immense experimental progress in the ability to measure quantum

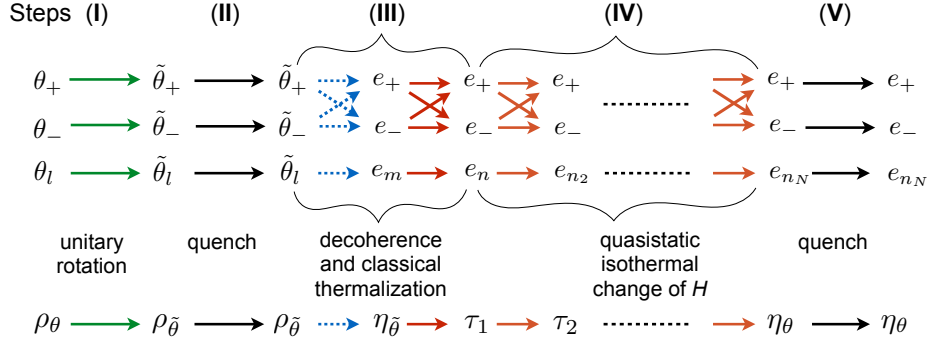


FIG. 2. **Pure-state qubit trajectories for the work extraction protocol.** Illustration of the evolution of the qubit during the work protocol on the trajectory level and on the density matrix level, cf. Fig. 1. The qubit’s trajectories are deterministic during Steps (I) (unitary, green arrows), (II) (quench, black arrows), and (V) (quench, black arrows), i.e. they take one state to a unique other state. In contrast, during the decoherence part in Step (III) (blue dashed arrows) the qubit stochastically jumps from one of the states $|\tilde{\theta}_\pm\rangle$ to one of the energy eigenstates $|e_\pm\rangle$, thus losing any quantum coherence in an irreversible manner. During the classical thermalization part in Step (III) (red arrows) the qubit stochastically jumps from one of the energy eigenstates to another energy eigenstate, thus losing any classical non-thermality in an irreversible manner. The qubit’s trajectories during the classical quasistatic isothermal change of H (Step (IV), orange arrows), are stochastic but reversible, due to infinitely small thermalizations taking place throughout.

states with high efficiency has enabled the observation of individual jumps in photon number, and more recently the tracking of single quantum trajectories of superconducting qubits [65–68]. The natural set of quantum trajectories is a function of how the system is measured, and various quantum trajectory sets have been discussed in the literature each corresponding to different measurement setups: the so-called “unravellings” [69, 70]. Averaging the system’s pure states over many experimental runs then gives back the density matrix describing the system’s mixed state, whose evolution is governed by completely positive, trace preserving maps, also known as a quantum channel. Using the methods of quantum stochastic thermodynamics we here access a system’s fluctuations in work, heat and entropy production, when quantum coherences are involved and irreversibility occurs. This allows us to expose the microscopic links between irreversibility and energetic exchanges in the quantum regime.

We here use “eigenstate trajectories” that describe a system that travels through a sequence of eigenstates of its time-local density operators. Namely, the system is measured at instances in time $j = 1, 2, \dots$ in its instantaneous eigenbases of the states ρ_j that are assumed to be known e.g. from a master equation that describes the open system dynamics. We note that this is an idealized scenario as in general one does not know what the density operators ρ_j are and cannot guarantee to measure in the correct eigenbases. The eigenstate trajectories are analytically tractable, and provide a first convenient analytical tool to investigate the energetic footprints of irreversibility, as we will see below.

In the following we will work with the idealized eigenstate trajectories. The ensemble of trajectories $\{\Gamma\}$ taken by a quantum system (here a qubit) when undergoing the work extraction protocol outlined in the previous section can be

broken up into trajectories for each of the Steps, see Fig. 2. We will here focus on discussing the thermalization of the qubit in Step (III), for which the initial qubit density matrix $\rho_{\tilde{\theta}}$ can host coherences *coh* and classical non-thermality *nonth* at the point when it is brought in contact with the thermal bath. The trajectories for the full protocol are detailed in Appendix A.

The thermalization process in Step (III) may be described by the quantum channel $\Lambda(\rho) := \text{tr}_{\mathcal{B}}[\mathcal{V}(\rho \otimes \tau_{\mathcal{B}})\mathcal{V}^\dagger]$ where $\tau_{\mathcal{B}} := \exp(-H_{\mathcal{B}}/k_{\mathcal{B}}T)/Z_{\mathcal{B}}$ is the initial thermal state of the bath with Hamiltonian $H_{\mathcal{B}}$ and partition function $Z_{\mathcal{B}}$, and \mathcal{V} is a unitary operator that commutes with $H_1 + H_{\mathcal{B}}$, hence Λ is a “thermal operation” [71–73]. Since Λ shall here be a fully thermalizing map we require that $\Lambda(\rho) = \tau_1$ for all ρ . This map exists, for example, when the bath is chosen as an infinite ensemble of identical particles, each with the same Hamiltonian as the system, and with \mathcal{V} implementing a sequence of partial swaps between the system and each bath particle [74]. Minimal trajectories for the thermalization process can now be constructed as $\Gamma_{(l,n)}^{(\text{III})} \equiv |\tilde{\theta}_l\rangle \mapsto |e_n\rangle$, see Fig. 2. The probability of this transfer to occur is $P(\Gamma_{(l,n)}^{(\text{III})}) = \langle \tilde{\theta}_l | \rho_{\tilde{\theta}} | \tilde{\theta}_l \rangle \langle e_n | \Lambda(|\tilde{\theta}_l\rangle\langle \tilde{\theta}_l|) | e_n \rangle$, which is obtained by first projectively measuring the system with respect to the eigenbasis $|\tilde{\theta}_l\rangle$ of $\rho_{\tilde{\theta}}$, then applying the thermalization channel Λ , and finally measuring the system with respect to the eigenbasis $|e_n\rangle$ of τ_1 . Since \mathcal{V} commutes with the total Hamiltonian while $\tau_{\mathcal{B}}$ commutes with the bath Hamiltonian, it can be shown (see Theorem 1 in [75]) that $\langle e_n | \Lambda(|\tilde{\theta}_l\rangle\langle \tilde{\theta}_l|) | e_n \rangle = \sum_m |\langle e_m | \tilde{\theta}_l \rangle|^2 \langle e_n | \Lambda(|e_m\rangle\langle e_m|) | e_n \rangle$, where $|e_m\rangle$ are eigenstates of the system Hamiltonian H_1 .

We may therefore “augment” our trajectories by project-

ing the system onto the energy basis $|e_m\rangle$ first before letting it thermalize classically. Such an augmentation was also performed in [35]. The augmented trajectories are denoted $\Gamma_{(l,m,n)}^{(\text{III})} \equiv |\tilde{\theta}_l\rangle \mapsto |e_m\rangle \mapsto |e_n\rangle$, with probabilities

$$P\left(\Gamma_{(l,m,n)}^{(\text{III})}\right) = \langle \tilde{\theta}_l | \rho_{\tilde{\theta}} | \tilde{\theta}_l \rangle | \langle e_m | \tilde{\theta}_l \rangle |^2 \langle e_n | \tau_1 | e_n \rangle. \quad (9)$$

It can be shown that the minimal trajectories $\Gamma_{(l,n)}^{(\text{III})}$ and the augmented trajectories $\Gamma_{(l,m,n)}^{(\text{III})}$ are thermodynamically equivalent, as they result in the same entropy production [35]. However, the augmented trajectories have the benefit of naturally splitting into a **decoherence trajectory** $\Gamma_{(l,m)}^q \equiv |\tilde{\theta}_l\rangle \mapsto |e_m\rangle$, followed by a **classical thermalization trajectory** $\Gamma_{(m,n)}^{\text{cl}} \equiv |e_m\rangle \mapsto |e_n\rangle$, as depicted in Fig. 2. Their probabilities to occur are

$$P\left(\Gamma_{(l,m)}^q\right) = \sum_n P\left(\Gamma_{(l,m,n)}^{(\text{III})}\right) = \langle \tilde{\theta}_l | \rho_{\tilde{\theta}} | \tilde{\theta}_l \rangle | \langle e_m | \tilde{\theta}_l \rangle |^2, \quad (10)$$

and

$$P\left(\Gamma_{(m,n)}^{\text{cl}}\right) = \sum_l P\left(\Gamma_{(l,m,n)}^{(\text{III})}\right) = \langle e_m | \eta_{\tilde{\theta}} | e_m \rangle \langle e_n | \tau_1 | e_n \rangle, \quad (11)$$

respectively. Here $\Gamma_{(l,m)}^q$ are the trajectories the system undertakes as it undergoes the decoherence process $\rho_{\tilde{\theta}} \mapsto \eta_{\tilde{\theta}}$, while $\Gamma_{(m,n)}^{\text{cl}}$ are the trajectories that the system undertakes as it undergoes the classical thermalization process $\eta_{\tilde{\theta}} \mapsto \tau_1$.

IV. Stochastic quantum entropy production

Within quantum stochastic thermodynamics the entropy production along a quantum trajectory Γ is

$$s_{\text{irr}}(\Gamma) := k_B \log \frac{P(\Gamma)}{P^*(\Gamma^*)}, \quad (12)$$

exposing the entropy production's microscopic origin as the imbalance between the probabilities $P(\Gamma)$ and $P^*(\Gamma^*)$ of a forward trajectory Γ and its corresponding backward trajectory Γ^* , respectively [38, 63]. As shown in Appendix A, the stochastic entropy production for the thermalization Step (III) can be expressed as

$$s_{\text{irr}}\left(\Gamma^{(\text{III})}\right) = s_{\text{irr}}^{\text{qu}}\left(\Gamma_{(l,m)}^q\right) + s_{\text{irr}}^{\text{cl}}\left(\Gamma_{(m,n)}^{\text{cl}}\right), \quad (13)$$

which is the sum of a *stochastic quantum entropy production*,

$$s_{\text{irr}}^{\text{qu}}\left(\Gamma_{(l,m)}^q\right) = k_B \log \frac{\langle \tilde{\theta}_l | \rho_{\tilde{\theta}} | \tilde{\theta}_l \rangle}{\langle e_m | \eta_{\tilde{\theta}} | e_m \rangle}, \quad (14)$$

and a *stochastic classical entropy production*,

$$s_{\text{irr}}^{\text{cl}}\left(\Gamma_{(m,n)}^{\text{cl}}\right) = k_B \log \frac{\langle e_m | \eta_{\tilde{\theta}} | e_m \rangle}{\langle e_m | \tau_1 | e_m \rangle}. \quad (15)$$

Since the probability of the augmented trajectories, $P\left(\Gamma_{(l,m,n)}^{(\text{III})}\right)$, gives $P\left(\Gamma_{(l,m)}^q\right)$ and $P\left(\Gamma_{(m,n)}^{\text{cl}}\right)$ as marginals (see Eq. (10) and Eq. (11)), the average entropy

production in Step (III) can also be split into an average quantum entropy production $\langle s_{\text{irr}}^{\text{qu}} \rangle_{\Gamma^q}$, and an average classical entropy production, $\langle s_{\text{irr}}^{\text{cl}} \rangle_{\Gamma^{\text{cl}}}$. One finds, see Appendix A, that each of these averages reduces to a relative entropy between two pairs of system states,

$$\langle s_{\text{irr}}^{\text{qu}} \rangle_{\Gamma^q} = \sum_{l,m} P\left(\Gamma_{(l,m)}^q\right) s_{\text{irr}}^{\text{qu}}\left(\Gamma_{(l,m)}^q\right) = k_B D[\rho_{\tilde{\theta}} \| \eta_{\tilde{\theta}}], \quad (16)$$

$$\langle s_{\text{irr}}^{\text{cl}} \rangle_{\Gamma^{\text{cl}}} = \sum_{m,n} P\left(\Gamma_{(m,n)}^{\text{cl}}\right) s_{\text{irr}}^{\text{cl}}\left(\Gamma_{(m,n)}^{\text{cl}}\right) = k_B D[\eta_{\tilde{\theta}} \| \tau_1]. \quad (17)$$

This shows that the relative entropies $D[\rho_{\tilde{\theta}} \| \eta_{\tilde{\theta}}]$ and $D[\eta_{\tilde{\theta}} \| \tau_1]$, which geometrically link density matrices, are physically meaningful as the average entropy productions associated with the evolution of the quantum system along ensembles of quantum trajectories. The two separate contributions to the entropy production arise because the qubit has two distinct non-equilibrium features, *coh* and *nonth*. Each is irreversibly removed when the qubit is brought into contact with the thermal bath and undergoes decoherence trajectories followed by classical thermalization trajectories. Moreover, we show in Appendix A that the average entropy production for the full protocol reduces to $\langle s_{\text{irr}}^{\text{qu}} \rangle_{\Gamma^q} + \langle s_{\text{irr}}^{\text{cl}} \rangle_{\Gamma^{\text{cl}}}$ in the limit where Step (IV) becomes a quasistatic process. I.e. in this limit the average entropy production for the full protocol coincides with the average entropy production for the thermalization step alone. Also in Appendix A we provide expressions for the variances of the two entropy productions.

V. Classical and quantum heat distributions

Having introduced the quantum decoherence and classical thermalization trajectories, $\Gamma_{(l,m)}^q$ and $\Gamma_{(m,n)}^{\text{cl}}$, respectively, we now analyze the energetic fluctuations in Step (III) associated with each source of irreversibility for the thermalization with the bath. Since there is no external control in Step (III), such as a change of Hamiltonian, no work is done on the system and hence the energetic change of the system consists entirely of heat. But since we identified two contributions to irreversibility, namely quantum decoherence and classical thermalization, it stands to reason that we should obtain two types of heat [36, 49].

The microscopic mechanisms associated with classical thermalization of the system with the bath are the quantum jumps from $|e_m\rangle$ to $|e_n\rangle$ with $m, n \in \{\pm\}$, which give rise to energetic fluctuations. The heat the qubit *absorbs* from the bath is

$$Q_{\text{cl}}\left(\Gamma_{(m,n)}^{\text{cl}}\right) = \frac{\hbar\omega_1}{2} (n - m), \quad (18)$$

which is the standard classical stochastic heat. Since the classical thermalization jumps are between well-defined quantum energy states, these fluctuations take one of the quantized values $-\hbar\omega_1, 0$, or $+\hbar\omega_1$. The probability of observing each value of stochastic classical heat is given by Eq. (11).

On the other hand, the microscopic mechanisms associated with decoherence are the quantum jumps from $|\tilde{\theta}_l\rangle$ to

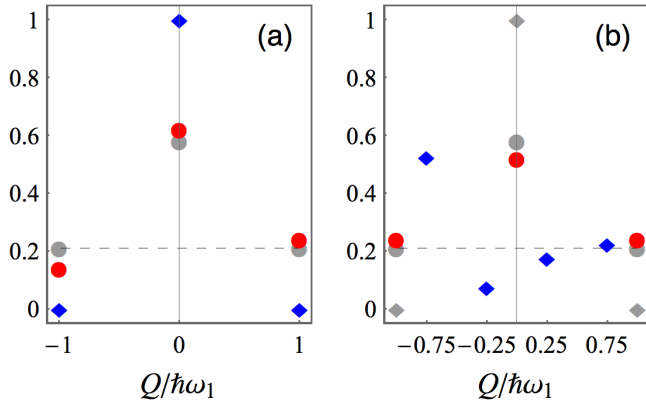


FIG. 3. **Heat distributions for thermalization Step (III)**. Histograms of classical heat Q_{cl} (red circles) and quantum heat Q_{qu} (blue squares) for (a) an initial state $\rho_{\bar{\theta}}$ that hosts classical non-thermality: $\text{nonth}(\rho_{\bar{\theta}}) = \log(0.2/0.3)$ and $\text{coh}(\rho_{\bar{\theta}}) = 0$, and for (b) an initial state $\rho_{\bar{\theta}}$ that hosts quantum non-thermality: $\text{coh}(\rho_{\bar{\theta}}) = \sin^2(\pi/6) = 1/4$ and $\text{nonth}(\rho_{\bar{\theta}}) = 0$. For comparison, grey circles and grey diamonds in both panels show the classical and quantum heat histograms, respectively, for when Step (III) is fully reversible, i.e. $\rho_{\bar{\theta}} = \tau_1$ and hence $\text{coh}(\rho_{\bar{\theta}}) = 0 = \text{nonth}(\rho_{\bar{\theta}})$. Note that, even then the system can exchange heat with the bath leading to a classical heat distribution with non-zero but symmetrical values (dashed line) that give a zero average classical heat. In (a) the only quantum heat value with non-zero probability is 0 (no quantum heat when thermalising a classical state), while in (b) four non-trivial quantum heat values occur since $\text{coh}(\rho_{\bar{\theta}}) \neq 0$.

$|e_m\rangle$, which give rise to energetic fluctuations of the system that are entirely quantum mechanical. The system's energy increase due to decoherence is

$$Q_{\text{qu}}(\Gamma_{(l,m)}^{\text{q}}) = \frac{\hbar\omega_1}{2} m - \langle \tilde{\theta}_l | H_1 | \tilde{\theta}_l \rangle, \quad (19)$$

and arises purely due to the loss of the system's initial coherences due to projective energy measurements. It has no classical counterpart and is hence referred to as *quantum heat* [36, 49]. The energetic fluctuations for these jumps take four values $\frac{\hbar\omega_1}{2}(m - l \cos \tilde{\theta})$ for $l, m \in \{\pm 1\}$. Contrary to the classical stochastic heat which has fixed quantized values given by the Hamiltonian H_1 alone, the stochastic quantum heat's values vary as a function of the eigenbasis of the initial state $\rho_{\bar{\theta}}$. The probability of these quantum heat values to be realised is given by Eq. (10). When the initial state has no quantum coherences ($\tilde{\theta} = 0 \rightarrow \text{coh}(\rho_{\bar{\theta}}) = 0$) the only realised value of the stochastic quantum heat is 0, i.e. in the absence of coherences, decoherence has no effect on the system's state and no energetic fluctuations result from it. Fluctuations of the quantum heat take place as soon as $\text{coh}(\rho_{\bar{\theta}}) \neq 0$. Histograms of the classical stochastic heat Q_{cl} and the quantum heat Q_{qu} are shown in Fig. 3(a) and 3(b) for initial states $\rho_{\bar{\theta}}$ that have only classical non-thermality while $\text{coh} = 0$, and states that have only coherences while $\text{nonth} = 0$, respectively.

Finally, Step (IV) also incurs classical heat. We do not discuss this contribution here, as the stochastic thermo-

dynamic description is well established for heat exchanges during this classical quasistatic isothermal process [58, 59].

VI. Heat footprints of classical and quantum irreversibility

We are now ready to discuss the energetic footprints of irreversibility in the quantum regime. The energetic footprints of classical entropy production during Step (III) are made immediately apparent from the stochastic equation (15) which, in conjunction with the classical heat value given by Eq. (18), can be re-expressed as

$$s_{\text{irr}}^{\text{cl}}(\Gamma_{(m,n)}^{\text{cl}}) = k_B \log \frac{\langle e_m | \eta_{\bar{\theta}} | e_m \rangle}{\langle e_n | \tau_1 | e_n \rangle} - \frac{Q_{\text{cl}}(\Gamma_{(m,n)}^{\text{cl}})}{T}. \quad (20)$$

When averaged over the classical thermalization trajectories $\Gamma_{(m,n)}^{\text{cl}}$, the above expression links the average absorbed heat $\langle Q_{\text{cl}} \rangle$ to the average entropy production $\langle s_{\text{irr}}^{\text{cl}} \rangle$ as

$$\langle s_{\text{irr}}^{\text{cl}} \rangle = k_B (S_{\text{vN}}(\tau_1) - S_{\text{vN}}(\eta_{\bar{\theta}})) - \frac{\langle Q_{\text{cl}} \rangle}{T}. \quad (21)$$

This thermodynamic equality, going back to Clausius, is the well-known energetic footprint of entropy production in the classical regime. It can be used to define the irreversibly dissipated heat,

$$\begin{aligned} \langle Q_{\text{diss}}^{\text{sur}} \rangle &:= -\langle Q_{\text{cl}} \rangle + T \Delta S_{\text{cl}}, \\ &= T \langle s_{\text{irr}}^{\text{cl}} \rangle = k_B T D[\eta_{\bar{\theta}} \| \tau_1] \geq 0, \end{aligned} \quad (22)$$

which is positive whenever the energetic difference between the entropy change, $\Delta S_{\text{cl}} = k_B (S_{\text{vN}}(\tau_1) - S_{\text{vN}}(\eta_{\bar{\theta}}))$, multiplied by bath temperature T , and the absorbed heat $\langle Q_{\text{cl}} \rangle$ is non-zero. This occurs when the entropy production $\langle s_{\text{irr}}^{\text{cl}} \rangle$ is non-zero, which in turn arises when the process is irreversible, see (12). In other words, the energetic footprint of non-zero $\langle Q_{\text{diss}}^{\text{sur}} \rangle$ gives thermodynamic testament to the arrow of time.

Meanwhile, the stochastic quantum entropy production $s_{\text{irr}}^{\text{qu}}(\Gamma_{(l,m)}^{\text{q}})$ in Eq. (14) is given purely by a stochastic quantum entropy change and does not appear to involve any contributions from the stochastic quantum heat Q_{qu} whatsoever. When averaged over all quantum decoherence trajectories, the quantum heat in fact vanishes, see Appendix B,

$$\langle Q_{\text{qu}} \rangle_{\Gamma^{\text{q}}} = 0, \quad (23)$$

while the average quantum entropy production can formally be rewritten as

$$\langle s_{\text{irr}}^{\text{qu}} \rangle = k_B (S_{\text{vN}}(\eta_{\bar{\theta}}) - S_{\text{vN}}(\rho_{\bar{\theta}})) - \frac{1}{T} \langle Q_{\text{qu}} \rangle. \quad (24)$$

This quantum thermodynamic equality shows that the energetic footprint of quantum entropy production, i.e. a fixed relationship between average heat absorption and average entropy production, is mute in the quantum regime. This indicates a fundamental difference in how quantum and classical heat relate to the entropy production.

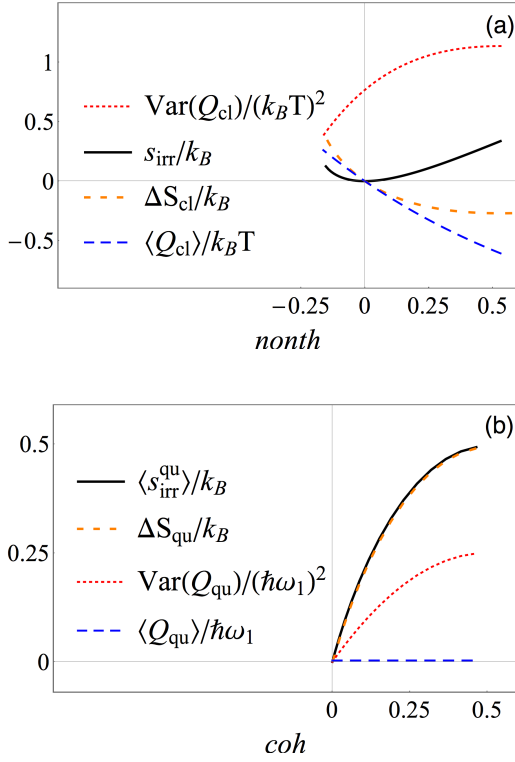


FIG. 4. **Heat footprint of irreversibility for Step (III).**

(a) Classical entropy production $\langle s_{\text{irr}}^{\text{cl}} \rangle$ plus the absorbed heat divided by the temperature $\langle Q_{\text{cl}} \rangle / T$ gives the entropy change ΔS_{cl} for any classical non-thermality parameter $\text{nonth}(\eta_{\bar{\theta}})$. With increasing nonth the entropy production $\langle s_{\text{irr}}^{\text{cl}} \rangle$ first decreases and then increases, while the variance of the classical heat, $\text{Var}(Q_{\text{cl}})$, increases monotonously with nonth . Positive (negative) non-thermality nonth corresponds to a lower (higher) ground state population in $\eta_{\bar{\theta}}$ than that of the thermal state τ_1 , corresponding to a down (up) red arrow in Fig. 1. Qubit spacing vs thermal energy ($\hbar\omega_1/k_B T$) is here set such that $q_1 = \langle e_- | \tau_1 | e_- \rangle = 0.85$ while $p \in [0.5, 1]$. (b) Quantum entropy production $\langle s_{\text{irr}}^{\text{qu}} \rangle$ plus zero average quantum heat $\langle Q_{\text{qu}} \rangle$ equals the entropy change ΔS_{qu} for any quantum coherence parameter coh of initial states $\rho_{\bar{\theta}}$. Also shown is the quantum heat variance $\text{Var}(Q_{\text{qu}})$ in natural units $(\hbar\omega_1)^2$. Both, $\text{Var}(Q_{\text{qu}})$ and $\langle s_{\text{irr}}^{\text{qu}} \rangle$, increase monotonously as coh tends to its maximum value of 0.5. Initial state mixing probability is here set to $p = 0.95$ while $\theta \in [0, \pi/2]$.

While *prima facie* Eq. (14) and Eq. (24) seem to suggest that the quantum entropy production is completely dissociated from quantum heat, such a conclusion is premature. Indeed, on closer examination we discover that the average quantum entropy production $\langle s_{\text{irr}}^{\text{qu}} \rangle$ is correlated with the fluctuations in quantum heat, as quantified by its variance, $\text{Var}(Q_{\text{qu}})$. In particular, for a qubit system, we show explicitly that both $\langle s_{\text{irr}}^{\text{qu}} \rangle$ and $\text{Var}(Q_{\text{qu}})$ are monotonically increasing functions of the coherence coh of the state $\rho_{\bar{\theta}}$ with respect to the Hamiltonian H_1 .

This property can be seen by straightforward evaluation of the quantum heat variance, see Appendix C,

$$\text{Var}(Q_{\text{qu}}) = \left(\frac{\hbar\omega_1}{2} \right)^2 (1 - (1 - 2 \text{coh}(\rho_{\bar{\theta}}))^2), \quad (25)$$

which monotonically increases as coh ranges from 0 to 1/2. As for $\langle s_{\text{irr}}^{\text{qu}} \rangle$, note that the eigenvalues of $\eta_{\bar{\theta}}$ can be arranged in the vector $\mathbf{r}_{\text{coh}} := (r_{\bar{\theta}}, 1 - r_{\bar{\theta}})$, where $r_{\bar{\theta}} = p(1 - \text{coh}(\rho_{\bar{\theta}})) + (1 - p)\text{coh}(\rho_{\bar{\theta}})$, see Eq. (5) and Eq. (7). As coh increases, $\text{coh}_2 \geq \text{coh}_1$, the eigenvalue $r_{\bar{\theta}}$ will decrease making $\mathbf{r}_{\text{coh}_2}$ more mixed, i.e. $\mathbf{r}_{\text{coh}_1} \succ \mathbf{r}_{\text{coh}_2}$. It follows that $S_{\text{vN}}(\eta_{\bar{\theta}})$, and hence $\langle s_{\text{irr}}^{\text{qu}} \rangle$, monotonically increase with coh [76, 77].

Fig. 4 puts in perspective the two drastically different energetic footprints of irreversibility in the classical and quantum regime. On the well-known classical side, see Fig. 4a, the average entropy production $\langle s_{\text{irr}}^{\text{cl}} \rangle$ is equal to the difference between the fixed entropy change ΔS_{cl} associated with the transfer $\eta_{\bar{\theta}} \rightarrow \tau_1$, and an absorbed heat $\langle Q_{\text{cl}} \rangle$ when this transfer is achieved by an irreversible thermalization process, divided by the temperature T . The classical heat footprint $\langle Q_{\text{cl}} \rangle$ scales as the thermal energy $k_B T$, an energy scale set by the temperature of the bath that thermalizes the qubit. The more non-thermal the initial (diagonal) qubit state $\eta_{\bar{\theta}}$ is, the more irreversibility will occur during its thermalization. Hence the classical entropy production $\langle s_{\text{irr}}^{\text{cl}} \rangle$ increases as the classical non-thermality parameter $\text{nonth}(\eta_{\bar{\theta}})$ deviates from 0. Note, however, that the entropy production is *not* a monotonic function of $\text{nonth}(\eta_{\bar{\theta}})$, since it decreases as $\text{nonth}(\eta_{\bar{\theta}})$ approaches zero from below.

On the quantum side, see Fig. 4b, the average entropy production $\langle s_{\text{irr}}^{\text{qu}} \rangle$ equals the entropy change $\Delta S_{\text{qu}} = k_B(S_{\text{vN}}(\eta_{\bar{\theta}}) - S_{\text{vN}}(\rho_{\bar{\theta}}))$ associated with the decoherence $\rho_{\bar{\theta}} \rightarrow \eta_{\bar{\theta}}$ and does not link to an absorbed quantum heat $\langle Q_{\text{qu}} \rangle$, as this is always zero. However, both $\langle s_{\text{irr}}^{\text{qu}} \rangle$ and the quantum heat fluctuations $\text{Var}(Q_{\text{qu}})$ monotonously increase with the coherence parameter $\text{coh}(\rho_{\bar{\theta}})$, showing an implicit link between entropy production and quantum heat for quantum decoherence processes. This behaviour differs from the classical counterpart, where the classical entropy production first drops and then increases again with increasing nonth , see Fig. 4a, while the classical heat variance increases monotonically with nonth , implying a non-monotonous relationship between $\langle s_{\text{irr}}^{\text{cl}} \rangle$ and $\text{Var}(Q_{\text{cl}})$. Finally, we remark that unlike the classical case, the heat footprint does not scale with temperature but with the system energy gap, here $\hbar\omega_1$, an energy scale set by the quantum character of the system rather than the thermodynamics implied by the bath.

For general quantum systems (not qubits) coh as defined in Eq. (7) is not a good measure of coherence. However, one can quantify the coherence in a general state ρ , with reference to Hamiltonian H , by the relative entropy of coherence $D[\rho||\eta]$ [78]. Since this is simply $\langle s_{\text{irr}}^{\text{qu}} \rangle / k_B$ as ρ decoheres to η , it trivially follows that the quantum entropy production will always be a monotonic function of coherence. However, proving that the quantum heat variance also increases monotonously with coherence remains an open question. What one can show for general quantum systems, is that the variance of the quantum heat is bounded, see Appendix B, as

$$\Delta(H, \rho) \geq \text{Var}(Q_{\text{qu}}) \geq I_{\alpha}(H, \rho), \quad (26)$$

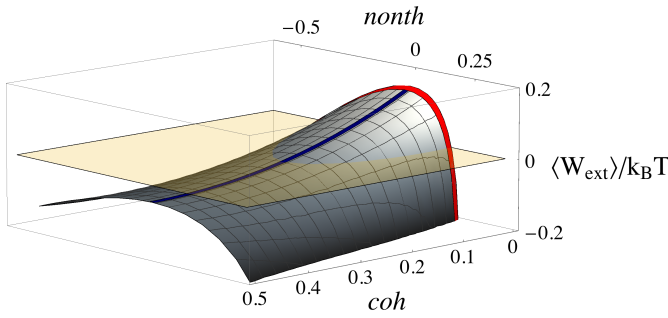


FIG. 5. **Average work extraction as a function of coh and $nonth$.** Work (grey) for the full protocol is optimal when neither quantum coherence nor classical non-thermality is present, i.e. $coh = 0 = nonth$, and the protocol is run reversibly [27]. $\langle W_{\text{ext}} \rangle$ decreases monotonously with increasing $coh(\rho_{\bar{\theta}})$ (blue line for $nonth = 0$) and increasing and decreasing $nonth(\rho_{\bar{\theta}})$ (red line for $coh = 0$). At large deviations from the reversible protocol, $\langle W_{\text{ext}} \rangle$ becomes negative (crosses yellow plane at zero) and work would need to be invested to run the protocol. Parameter choices for initial qubit state ρ_{θ} are $p = 0.8$ and $\theta = \pi/3$.

for $\alpha \in (0, 1)$, where $\Delta(H, \rho)$ is the energy variance $\Delta(H, \rho) := \text{tr}[H^2 \rho] - \text{tr}[H \rho]^2$ and $I_{\alpha}(H, \rho)$ is the set of Wigner-Yanase-Dyson skew informations

$$I_{\alpha}(H, \rho) := \text{tr}[H^2 \rho] - \text{tr}[H \rho^{\alpha} H \rho^{1-\alpha}] \quad (27)$$

of the observable H in the state ρ [79–81]. While the energy variance $\Delta(H, \rho)$ includes quantum and classical uncertainty, the skew information $I_{\alpha}(H, \rho)$ measures purely quantum contributions to the variance. Inequality (26) shows that all quantum uncertainty, and some contribution from the classical uncertainty, limit the magnitude of quantum heat variance $\text{Var}(Q_{\text{qu}})$. It has been suggested that the skew information can act as a measure for coherence [82]. Therefore, for general quantum systems, we can conclude that the average quantum entropy production $\langle s_{\text{irr}}^{\text{qu}} \rangle$ as well as the lower bounds $I_{\alpha}(H, \rho)$ to the quantum heat variance $\text{Var}(Q_{\text{qu}})$ monotonically increase with coherence.

The skew information is also intimately linked to the resource theory of asymmetry [83–85] as it quantifies how asymmetric a quantum state ρ is with reference to unitary representations of a symmetry group G , generated by the self-adjoint operator H . It has been shown [86] that the extractable work from asymmetric states will be reduced if the work extraction process obeys symmetry constraints; in our protocol, the process in Steps (III) to (V) is symmetric with respect to unitary evolutions generated by H_1 , and so the more asymmetric $\rho_{\bar{\theta}}$ is with respect to H_1 , the less work can be extracted from it.

VII. Fundamental bounds for work extraction

Finally, we check the validity of the work footprint of entropy production, Eq. (2), in the quantum regime. Here it suffices to demonstrate the link to the work average only, higher moments of work can straightforwardly be analysed using quantum trajectories.

The average energy change over the entire protocol vanishes by construction, and equals the average heat absorbed by the system minus the average work extracted from the system throughout the entire protocol,

$$0 = \text{tr}[(\eta_{\theta} - \rho_{\theta}) H_0] = \Delta U^{\text{prot}} = \langle Q^{\text{prot}} \rangle - \langle W_{\text{ext}} \rangle.$$

Hence the work averaged over the entire protocol's trajectories is

$$\begin{aligned} \langle W_{\text{ext}} \rangle &= \langle Q_{\text{qu}} \rangle_{\Gamma^{\text{q}}} + \langle Q_{\text{cl}} \rangle_{\Gamma^{\text{cl}}} + \langle Q_{\text{cl}}^{(\text{IV})} \rangle_{\Gamma^{(\text{IV})}} \quad (28) \\ &= 0 - T \langle s_{\text{irr}}^{\text{cl}} \rangle + T \Delta S_{\text{cl}} + T \Delta S^{(\text{IV})}, \end{aligned}$$

where we have assumed quasistatic isothermal trajectories $\Gamma^{(\text{IV})}$ in Step (IV) with $\langle s_{\text{irr}}^{(\text{IV})} \rangle = 0$ and

$$\langle Q_{\text{cl}}^{(\text{IV})} \rangle_{\Gamma^{(\text{IV})}} = T \Delta S^{(\text{IV})} = T k_B (S_{\text{vN}}(\eta_{\theta}) - S_{\text{vN}}(\tau_1)).$$

Substituting the entropy change across the entire protocol

$$\Delta S^{\text{prot}} = \Delta S_{\text{qu}} + \Delta S_{\text{cl}} + \Delta S^{(\text{IV})},$$

and using $\Delta F^{\text{prot}} = -T \Delta S^{\text{prot}} = -k_B T (S_{\text{vN}}(\eta_{\theta}) - S_{\text{vN}}(\rho_{\theta}))$ since $\Delta U^{\text{prot}} = 0$, the result is

$$\langle W_{\text{ext}} \rangle = -\Delta F^{\text{prot}} - T (\langle s_{\text{irr}}^{\text{cl}} \rangle + \langle s_{\text{irr}}^{\text{qu}} \rangle). \quad (29)$$

Clearly, the optimum work value $-\Delta F^{\text{prot}}$ is obtained when neither classical nor quantum entropy production are present and the process is run fully reversibly, as discussed in Ref. [27]. Equation (29) further shows that the classical and quantum entropy productions limit work extraction in a similar way. In addition to the classical entropy production $\langle s_{\text{irr}}^{\text{cl}} \rangle$, in the quantum regime the quantum entropy production $\langle s_{\text{irr}}^{\text{qu}} \rangle$, linked to the irreversible removal of coherences, reduces work extraction in a completely symmetrical manner, see Eq. (2). The footprint of irreversibility on work extraction is shown in Fig. 5, where $\langle W_{\text{ext}} \rangle$ is plotted as a function of the two parameters that give rise to irreversibility, the quantum coherence coh and classical non-thermality $nonth$ of the state $\rho_{\bar{\theta}}$ before thermal contact.

While work extraction is mathematically limited in a symmetrical manner, the physical mechanism is drastically different depending on if the irreversibility of the protocol is of classical or of quantum nature. In the classical regime the irreversibly dissipated heat $\langle Q_{\text{diss}}^{\text{sur}} \rangle$ is the physical cause of non-optimal work extraction and exactly compensates the non-recoverable work, i.e. the term $T \langle s_{\text{irr}}^{\text{cl}} \rangle = \langle Q_{\text{diss}}^{\text{sur}} \rangle$ in Eq. (29). This energetic footprint of irreversibility equals the average energy change of the qubit during the irreversible thermalization step. But the quantum decoherence step does not give rise to any average energy change - the work extraction is here reduced solely because the system entropy increases, reducing the extracted work by a proportional amount $T \langle s_{\text{irr}}^{\text{qu}} \rangle = T \Delta S_{\text{qu}}$.

VIII. Discussion

The notion of irreversibility and how it affects heat and work exchanges is a core pillar of thermodynamics. This paper brings together several strands of recent research in

quantum thermodynamics, including stochastic thermodynamics and quantum work extraction protocols, to provide a comprehensive picture of when irreversibility arises in the quantum regime and details the ensuing energetic footprints of irreversibility. Specifically, we have shown that the geometric entropy production $D[\rho_{\delta}||\tau_1]$, which can be calculated using density matrices, can be understood as arising from the time-reversal asymmetry of quantum stochastic trajectories, Eq. (16) and Eq. (17), in a similar way to classical stochastic thermodynamics. Our arguments follow similar lines of reasoning as the recent work in [35]. In addition, the quantum trajectories allowed for a detailed assessment of work and heat exchanges of a quantum system that can host coherences. While reversible work extraction from quantum coherences has been found [27] to give an “average” work of $\langle W_{\text{ext}} \rangle^{\text{rev}} = -\Delta F^{\text{prot}}$, no distribution of work was provided with respect to which $\langle W_{\text{ext}} \rangle^{\text{rev}}$ is an “average”. Here we showed that quantum trajectories naturally give rise to heat as well as work distributions, for which moments, such as the work “average”, can be readily calculated. For the sake of brevity we have here obtained the average work from averaging over the heat distributions in (28), avoiding the need to explicitly construct the work distribution. By here including irreversible steps in the work extraction protocol, the reduction of work due to irreversibility has been quantified in Eq. (29). Understanding how imperfect experimental control, which leaves either quantum coherences, or classical non-thermality, or both present in a quantum system before thermal contact, reduces work extraction, is important for identifying experimental protocols that are optimal within realistic technical constraints.

While the first moments of heat and work coincide with the values obtained on the density matrix level, the trajectories approach allows access to higher moments of heat and work. This proved insightful for the discussion of the footprint of quantum irreversibility. We found that the average classical entropy production is linked to the surplus of dissipated heat, see Eq. (22), which is fully analogous to the classical regime, see Eq. (1). Conversely, no such link can be made in regards to quantum entropy production, see Eq. (24). Instead, we show that the quantum entropy production is correlated with the fluctuations in quantum heat. Specifically, for a general quantum system, the average quantum entropy production, and the lower bound of the quantum heat variance, monotonically increases with the initial state’s coherence, coh (see Eq. (26)). In the special case of qubits, we explicitly show that the variance in quantum heat also grows monotonously with the coherence. This footprint was hidden from view before as it cannot be

described on the density matrix level alone. By using the quantum trajectories approach we have here uncovered this energetic footprint for the first time. A comparable link does not exist in the classical regime where $\text{Var}(Q_{\text{cl}})$ grows monotonically with the initial state’s non-thermality nonth , but the classical entropy production $\langle s_{\text{irr}}^{\text{cl}} \rangle$ does not. It would be interesting to see if the same conclusions hold true when the eigenstate trajectories are replaced by experimentally measured trajectories and their probabilities, for which the analysis presented here can be implemented in an analogous manner.

Another open problem is to establish the relationship between quantum entropy production and the fluctuations in quantum heat for arbitrarily large quantum systems with states that may host degeneracy in their eigenvalues. On the one hand, the inequality in Eq. (26), which is valid for arbitrary dimensions, does not establish a monotonicity relationship between coherence and the variance in quantum heat – only the lower bound in the variance of quantum heat increases with coherence. On the other hand, when the system’s state has degeneracies, it will offer infinitely many spectral decompositions, and the corresponding quantum heat fluctuations will not be equivalent. Here a physical principle may need to be invoked to select a particular decomposition, such as including explicit projective measurements on the system before it undergoes decoherence with respect to the Hamiltonian.

Performing coherent manipulations of quantum systems requires $\hbar\omega_1 \gg k_B T$, so that the quantum energetic fluctuations due to quantum irreversibility largely overcome the mean energetic exchanges due to classical entropy production. Therefore this energetic footprint is expected to play an important role in the energetic assessment of quantum control operating at low temperature, including quantum processors in cryostats.

Acknowledgments. We have the pleasure to thank Karen Hovhannisyanyan, Harry Miller, Cyril Elouard and Ian Ford for inspiring discussions. This research was supported in part by the COST network MP1209 “Thermodynamics in the quantum regime” and by the National Science Foundation under Grant No. NSF PHY-1748958. M.H.M. acknowledges support from EPSRC via Grant No. EP/P030815/1. A.A. acknowledges the Agence Nationale de la Recherche under the Research Collaborative Project “Qu-DICE” (ANR-PRC-CES47). J.A. acknowledges support from EPSRC (grant EP/R045577/1) and the Royal Society.

-
- [1] J. Goold, M. Huber, A. Riera, L. del Rio, and P. Skrzypczyk, *J. Phys. A* **49**, 143001 (2016).
 [2] J. Millen and A. Xuereb, *New J. Phys.* **18**, 011002 (2016).
 [3] S. Vinjanampathy and J. Anders, *Contemp. Phys.* **57**, 545 (2016).
 [4] F. Binder, L. A. Correa, C. Gogolin, J. Anders, and

- G. Adesso, eds., *Thermodynamics in the Quantum Regime*, Fundamental Theories of Physics, Vol. 195 (Springer International Publishing, Cham, 2018).
 [5] a. E. Allahverdyan, R. Balian, and T. M. Nieuwenhuizen, *Epl* **565**, 5 (2004).
 [6] J. Aberg and S. Information, *Nat. Commun.* **4**, 1925 (2013).

- [7] M. F. Frenzel, D. Jennings, and T. Rudolph, *Phys. Rev. E* **90**, 1 (2014).
- [8] M. Perarnau-Llobet, K. V. Hovhannisyán, M. Huber, P. Skrzypczyk, N. Brunner, and A. Acín, *Phys. Rev. X* **5**, 041011 (2015).
- [9] P. Skrzypczyk, A. J. Short, and S. Popescu, *Nat. Commun.* **5**, 4185 (2014).
- [10] M. Lostaglio, K. Korzekwa, D. Jennings, and T. Rudolph, *Phys. Rev. X* **5**, 1 (2015).
- [11] P. Ćwikliński, M. Studziński, M. Horodecki, and J. Oppenheim, *Phys. Rev. Lett.* **115**, 210403 (2015).
- [12] M. Lostaglio, D. Jennings, and T. Rudolph, *New J. Phys.* **19**, 043008 (2017).
- [13] M. T. Mitchison, M. P. Woods, J. Prior, and M. Huber, *New J. Phys.* **17**, 115013 (2015).
- [14] K. Korzekwa, M. Lostaglio, J. Oppenheim, and D. Jennings, *New J. Phys.* **18**, 23045 (2016).
- [15] A. Misra, U. Singh, S. Bhattacharya, and A. K. Pati, *Phys. Rev. A* **93**, 052335 (2016).
- [16] H. J. D. Miller and J. Anders, *New J. Phys.* **19**, 062001 (2017).
- [17] R. Uzdin, A. Levy, and R. Kosloff, *Entropy* **18**, 124 (2016).
- [18] N. H. Ying Ng, M. P. Woods, and S. Wehner, *New J. Phys.* **19**, 113005 (2017).
- [19] A. Streltsov, G. Adesso, and M. B. Plenio, *Rev. Mod. Phys.* **89**, 041003 (2017).
- [20] M. F. Frenzel, D. Jennings, and T. Rudolph, *New J. Phys.* **18**, 23037 (2016).
- [21] J. Klatzow, C. Weinzetl, P. M. Ledingham, J. N. Becker, D. J. Saunders, J. Nunn, I. A. Walmsley, R. Uzdin, and E. Poem, (2017), arXiv:1710.08716.
- [22] H. Kwon, H. Jeong, D. Jennings, B. Yadin, and M. S. Kim, (2017), arXiv:1711.03395.
- [23] M. H. Mohammady and J. Anders, *New J. Phys.* **19**, 113026 (2017).
- [24] Y. Morikuni, H. Tajima, and N. Hatano, *Phys. Rev. E* **95**, 032147 (2017).
- [25] R. Uzdin, *Phys. Rev. Appl.* **6**, 024004 (2016).
- [26] R. Uzdin, A. Levy, and R. Kosloff, *Phys. Rev. X* **5**, 031044 (2015).
- [27] P. Kammerlander and J. Anders, *Sci. Rep.* **6**, 22174 (2016).
- [28] P. Solinas and S. Gasparinetti, *Phys. Rev. A* **94**, 052103 (2016).
- [29] M. Lostaglio, D. Jennings, and T. Rudolph, *Nat. Commun.* **6**, 6383 (2015).
- [30] L. d. Rio, J. Aberg, R. Renner, O. Dahlsten, and V. Vedral, *Nature*, 61 (2011).
- [31] I. Callens, W. De Roeck, T. Jacobs, C. Maes, and K. Netočný, *Physica D* **187**, 383 (2004).
- [32] J. M. Horowitz and J. M. R. Parrondo, *New J. Phys.* **15** (2013), 10.1088/1367-2630/15/8/085028.
- [33] J. J. Alonso, E. Lutz, and A. Romito, *Phys. Rev. Lett.* **116**, 1 (2016).
- [34] G. Francica, J. Goold, and F. Plastina, (2017), arXiv:1707.06950.
- [35] J. P. Santos, L. C. Céleri, G. T. Landi, and M. Paternostro, *npj Quantum Information* **5**, 23 (2019).
- [36] C. Elouard, D. A. Herrera-Martí, M. Clusel, and A. Auffèves, *npj Quantum Information* **3**, 9 (2017).
- [37] C. Elouard, N. K. Bernardes, A. R. R. Carvalho, M. F. Santos, and A. Auffèves, *New J. Phys.* **19**, 103011 (2017).
- [38] G. Manzano, J. M. Horowitz, and J. M. R. Parrondo, *Phys. Rev. X* **8**, 031037 (2018).
- [39] S. K. Manikandan, C. Elouard, and A. N. Jordan, *Phys. Rev. A* **99**, 022117 (2019).
- [40] S. Deffner and E. Lutz, *Phys. Rev. Lett.* **107**, 1 (2011).
- [41] G. E. Crooks, *Phys. Rev. E* **60**, 2721 (1999).
- [42] U. Seifert, *Phys. Rev. Lett.* **95**, 040602 (2005).
- [43] U. Seifert, *Rep. Prog. Phys.* **75**, 126001 (2012).
- [44] M. Brunelli, L. Fusco, R. Landig, W. Wieczorek, J. Hoelscher-Obermaier, G. Landi, F. L. Semião, A. Ferraro, N. Kiesel, T. Donner, G. De Chiara, and M. Paternostro, *Phys. Rev. Lett.* **121**, 160604 (2018).
- [45] K. Ptaszyński and M. Esposito, *Phys. Rev. Lett.* **122**, 150603 (2019).
- [46] L. D. Landau and E. M. Lifshitz, *Statistical Physics: Volume 5 (Course of Theoretical Physics)* (Butterworth-Heinemann, 1980).
- [47] R. Balian, *From Microphysics to Macrophysics: volume 1* (Springer, 2007).
- [48] F. Weinhold, *Classical and Geometrical Theory of Chemical and Phase Thermodynamics* (Wiley, 2009).
- [49] C. Elouard, N. K. Bernardes, A. R. R. Carvalho, M. F. Santos, and A. Auffèves, *New J. Phys.* **19**, 103011 (2017).
- [50] M. H. Mohammady and A. Romito, (2018), arXiv:1809.09010.
- [51] L. Buffoni, A. Solfanelli, P. Verrucchi, A. Cuccoli, and M. Campisi, *Phys. Rev. Lett.* **122**, 070603 (2019).
- [52] J. Anders and V. Giovannetti, *New J. Phys.* **15** (2012), 10.1088/1367-2630/15/3/033022.
- [53] J. Gemmer and J. Anders, *New J. Phys.* **17**, 085006 (2015).
- [54] M. Esposito, K. Lindenberg, and C. V. den Broeck, *New J. Phys.* **12**, 013013 (2010).
- [55] G. Manzano, F. Plastina, and R. Zambrini, *Phys. Rev. Lett.* **121**, 120602 (2018).
- [56] S. Deffner and E. Lutz, *Phys. Rev. Lett.* **105**, 170402 (2010).
- [57] Excited state probabilities are fixed by the ground state probabilities for a qubit, for d -level systems higher level probabilities need to be included.
- [58] U. Seifert, *Eur. Phys. J. B* **64**, 423 (2008).
- [59] K. Sekimoto, *Stochastic Energetics* (Springer, 2010).
- [60] G. Manzano, J. M. Horowitz, and J. M. R. Parrondo, *Phys. Rev. E* **92**, 1 (2015), 1505.04201.
- [61] Y. Murashita, Z. Gong, Y. Ashida, and M. Ueda, (2017), arXiv:1705.06513.
- [62] P. Grangier and A. Auffèves, *Philos. Trans. Royal Soc. A* **376** (2018), 10.1098/rsta.2017.0322.
- [63] C. Elouard and M. H. Mohammady, *Thermodynamics in the Quantum Regime*, edited by F. Binder, L. A. Correa, C. Gogolin, J. Anders, and G. Adesso, *Fundamental Theories of Physics*, Vol. 195 (Springer International Publishing, Cham, 2018) pp. 363–393.
- [64] S. Haroche and J.-M. Raimond, *Exploring the Quantum: Atoms, Cavities, and Photons* (Oxford university press, 2006).
- [65] S. Gleyzes, S. Kuhr, C. Guerlin, J. Bernu, S. Deléglise, U. Busk Hoff, M. Brune, J. Raimond, and S. Haroche, *Nature* **446**, 297 (2007).
- [66] P. Campagne-Ibarcq, P. Six, L. Bretheau, A. Sarlette, M. Mirrahimi, P. Rouchon, and B. Huard, *Phys. Rev. X* **6**, 011002 (2016).
- [67] J. J. Alonso, E. Lutz, and A. Romito, *Phys. Rev. Lett.* **116**, 080403 (2016).
- [68] K. W. Murch, S. J. Weber, M. C., and S. I., *Nature* **502**, 211 (2013).
- [69] H. J. Carmichael, *Statistical Methods in Quantum Optics*

2: *Non-Classical Fields* (Springer, 2007).

- [70] S. Gammelmark and K. Mølmer, *Phys. Rev. A* **87**, 032115 (2013).
- [71] C. Perry, P. Ćwikliński, J. Anders, M. Horodecki, and J. Oppenheim, *Phys. Rev. X* **8**, 041049 (2018).
- [72] M. Lostaglio, Á. M. Alhambra, and C. Perry, *Quantum* **2**, 52 (2018).
- [73] N. Huei, Y. Ng, and M. P. Woods, *Thermodynamics in the Quantum Regime*, edited by F. Binder, L. A. Correa, C. Gogolin, J. Anders, and G. Adesso, *Fundamental Theories of Physics*, Vol. 195 (Springer International Publishing, Cham, 2018) pp. 625–650.
- [74] M. Ziman and V. Bužek, “Open system dynamics of simple collision models,” in *Quantum Dynamics and Information*, pp. 199–227.
- [75] M. Mohammady and A. Romito, *Universe* **5**, 46 (2019).
- [76] R. Bhatia, *Matrix Analysis* (Springer, 1997).
- [77] Y. Li and P. Busch, *J. Math. Anal. Appl.* **408**, 384 (2013).
- [78] T. Baumgratz, M. Cramer, and M. Plenio, *Phys. Rev. Lett.* **113**, 140401 (2014).
- [79] E. P. Wigner and M. M. Yanase, *Proc. Natl. Acad. Sci.* **49**, 910 (1963).
- [80] E. H. Lieb, *Adv. Math.* **11**, 267 (1973).
- [81] K. Yanagi, *J. Phys. Conf. Ser.* **201**, 012015 (2010).
- [82] It has been suggested [87] that $I_\alpha(H, \rho)$ can also act as a measure of coherence in ρ with reference to the observable H . However, this satisfies the monotonicity condition of coherence measures [78] only under the action of incoherent operations that are phase-insensitive [88] or, more precisely, are symmetric with respect to group actions generated by H : operations Φ such that $\Phi(e^{-itH} \rho e^{itH}) = e^{-itH} \Phi(\rho) e^{itH}$ [89]. The decoherence map $\Phi(\rho) = \eta$ trivially satisfies this condition.
- [83] M. Ahmadi, D. Jennings, and T. Rudolph, *New J. Phys.* **15**, 013057 (2013).
- [84] I. Marvian and R. W. Spekkens, *Nat. Commun.* **5**, 1 (2014).
- [85] R. Takagi, (2018), arXiv:1812.10453.
- [86] J. A. Vaccaro, F. Anselmi, H. M. Wiseman, and K. Jacobs, *Phys. Rev. A* **77**, 032114 (2008).
- [87] D. Girolami, *Phys. Rev. Lett.* **113**, 1 (2014).
- [88] S. Du and Z. Bai, *Ann. Phys.* **359**, 136 (2015).
- [89] I. Frérot and T. Roscilde, *Phys. Rev. B* **94**, 1 (2016).
- [90] S. Beigi and A. Gohari, *IEEE Trans. Inf. Theory* **60**, 7980 (2014).
- [91] C. T. Chubb, M. Tomamichel, and K. Korzekwa, *Quantum* **2**, 108 (2018).
- [92] K. Korzekwa, C. T. Chubb, and M. Tomamichel, *Phys. Rev. Lett.* **122**, 110403 (2019).

Appendix

A. Trajectories for the full work extraction protocol

We now introduce the full trajectories of the protocol, with expressions for their probabilities, and evaluate the stochastic entropy production associated with each trajectory. We shall show that the full entropy production can be split into entropy production terms associated for each step. Next, we show that the average entropy production for the full protocol reduces to the average entropy production for Step **(III)** in the limit that the evolution in Step **(IV)** becomes quasistatic. Finally, we evaluate the fluctuations in the entropy production during Step **(III)** of the protocol.

Recall that the work extraction protocol can be split as follows. Step **(I)**: unitary evolution $\rho_\theta \mapsto \rho_{\tilde{\theta}}$; Step **(II)**: Hamiltonian quench $H_0 \mapsto H_1$; Step **(III)**: decoherence $\rho_{\tilde{\theta}} \mapsto \eta_{\tilde{\theta}}$ followed by classical thermalization $\eta_{\tilde{\theta}} \mapsto \tau_1$; Step **(IV)**: quasistatic evolution $\tau_1 \mapsto \dots \mapsto \tau_N \equiv \eta_\theta$; and Step **(V)**: Hamiltonian quench $H_N \mapsto H_0$. Since Steps **(II)** and **(V)** are only Hamiltonian quenches, and do not alter the state, we shall not include these when constructing our trajectories.

Each thermalization process that the system undertakes is described by the channels $\Lambda_i : \rho \mapsto \text{tr}_{\mathcal{B}_i}[\mathcal{V}_i(\rho \otimes \tau_{\mathcal{B}_i})\mathcal{V}_i^\dagger]$, where $\mathcal{B}_1 \equiv \mathcal{B}$ and $\mathcal{V}_1 \equiv \mathcal{V}$ are the bath and unitary used in Step **(III)**, while $\mathcal{B}_2, \dots, \mathcal{B}_N$ and $\mathcal{V}_2, \dots, \mathcal{V}_N$ are the baths and unitaries used in Step **(IV)**. We shall decompose each thermalization channel into their Kraus operators $K_{\mu_i, \nu_i} := \sqrt{\langle \mu_i | \tau_{\mathcal{B}_i} | \mu_i \rangle} \langle \nu_i | \mathcal{V}_i | \mu_i \rangle$, where $|\mu_i\rangle$ and $|\nu_i\rangle$ are eigenstates of bath Hamiltonian $H_{\mathcal{B}_i}$, with energy eigenvalues $\epsilon_\mu(i)$ and $\epsilon_\nu(i)$, respectively. Such Kraus operators are constructed if, before and after the bath’s joint unitary evolution with the system, we subject it to projective energy measurements.

The full trajectory that the system takes during the protocol, therefore, can be expressed as

$$\Gamma = \Gamma_{(l, n_0, \dots, n_N), (\mu_1, \nu_1), (\mu_2, \nu_2), \dots, (\mu_N, \nu_N)}, \quad (\text{A1})$$

where $\Gamma_S := (l, n_0, \dots, n_N) \equiv |\theta_l\rangle \mapsto |\tilde{\theta}_l\rangle \mapsto |e_{n_0}\rangle \mapsto \dots \mapsto |e_{n_N}\rangle$ is the sequence of time-local eigenstates of the system during the protocol. Note that, here, we identify $n_0 \equiv m$ and $n_1 \equiv n$ as the eigenstate labels during Step **(III)**. The bath indices (μ_i, ν_i) merely indicate the sequence of energy measurement outcomes on the baths, and they only contribute to the probabilities of the system trajectories Γ_S . The probability of the trajectory Γ is evaluated to be

$$\begin{aligned} P(\Gamma) &= \langle \tilde{\theta}_l | \rho_{\tilde{\theta}} | \tilde{\theta}_l \rangle \| \mathcal{K}_\Gamma \|^2 \\ &= \langle \tilde{\theta}_l | \rho_{\tilde{\theta}} | \tilde{\theta}_l \rangle | \langle \tilde{\theta}_l | e_{n_0} \rangle |^2 \\ &\quad \times \prod_{i=1}^N \langle \mu_i | \tau_{\mathcal{B}_i} | \mu_i \rangle | \langle e_{n_i} \nu_i | \mathcal{V}_i | e_{n_{i-1}} \mu_i \rangle |^2, \quad (\text{A2}) \end{aligned}$$

where we have introduced the full Kraus operator for the protocol,

$$\mathcal{K}_\Gamma := \Pi[e_{n_N}] K_{\mu_N, \nu_N} \dots \Pi[e_{n_1}] K_{\mu_1, \nu_1} \Pi[e_{n_0}] \Pi[|\tilde{\theta}_l\rangle]. \quad (\text{A3})$$

Averaging over all the measurement outcomes on the bath,

meanwhile, yields the probabilities for the system-only trajectories Γ_S , given as

$$P(\Gamma_S) = \langle \tilde{\theta}_l | \rho_{\tilde{\theta}} | \tilde{\theta}_l \rangle |\langle \tilde{\theta}_l | e_{n_0} \rangle|^2 \prod_{i=1}^N \langle e_{n_i} | \tau_i | e_{n_i} \rangle. \quad (\text{A4})$$

Note that we may recover the probability for any sub-trajectory of the system by summing over all other indices of Eq. (A4). For example, summing over the indices of Steps **(I)** and **(IV)**, and the classical thermalization of Step **(III)**, the probabilities for the system's quantum decoherence trajectories $\Gamma_{(l,m)}^q$ are obtained as

$$\begin{aligned} \sum_{n_i > 0} P(\Gamma_S) &= \langle \tilde{\theta}_l | \rho_{\tilde{\theta}} | \tilde{\theta}_l \rangle |\langle \tilde{\theta}_l | e_{n_0} \rangle|^2 \\ &= P(\Gamma_{(l,m)}^q). \end{aligned} \quad (\text{A5})$$

Summing instead over the indices of Steps **(I)** and **(IV)**, and the quantum decoherence of Step **(III)**, the probabilities for the system's classical thermalization trajectories $\Gamma_{(m,n)}^{\text{cl}}$ are

$$\begin{aligned} \sum_{l, n_i > 1} P(\Gamma_S) &= \sum_l \langle \tilde{\theta}_l | \rho_{\tilde{\theta}} | \tilde{\theta}_l \rangle |\langle \tilde{\theta}_l | e_{n_0} \rangle|^2 \langle e_{n_1} | \tau_1 | e_{n_1} \rangle \\ &= \langle e_m | \eta_{\tilde{\theta}} | e_m \rangle \langle e_n | \tau_1 | e_n \rangle \\ &= P(\Gamma_{(m,n)}^{\text{cl}}). \end{aligned} \quad (\text{A6})$$

We may also reconstruct the full density operator for the system, at any point along the trajectory, see Fig. 2, by weighting the pure states by the total trajectory probabilities that include this term. For example, the average state after the decoherence process in Step **(III)** is indeed

$$\begin{aligned} &\sum_m |e_m\rangle \langle e_m| \sum_{l, n_1, \dots, n_N} P(\Gamma_S) \\ &= \sum_m |e_m\rangle \langle e_m| \langle e_m | \eta_{\tilde{\theta}} | e_m \rangle \\ &= \eta_{\tilde{\theta}}. \end{aligned} \quad (\text{A7})$$

The time-reversed trajectories can be defined by reversing the order of the protocol. Here we have Step **(IV)**: quasistatic reversed isothermal jumps $|e_{n_N}\rangle \mapsto \dots \mapsto |e_{n_1}\rangle$; Step **(III)** reversed thermalization $|e_{n_1}\rangle \mapsto |e_{n_0}\rangle$ followed by reversed decoherence $|e_{n_0}\rangle \mapsto |\tilde{\theta}_l\rangle$; and Step **(I)**: reversed unitary evolution $|\tilde{\theta}_l\rangle \mapsto |\theta_l\rangle$. Moreover, we shall consider the time-reversed thermalization maps $\Lambda_i^* : \rho \mapsto \text{tr}_{\mathcal{B}_i}[\mathcal{V}_i^\dagger(\rho \otimes \tau_{\mathcal{B}_i})\mathcal{V}_i]$. Note that the only difference between Λ_i and Λ_i^* is that we have applied the time reversal operation on the unitaries \mathcal{V}_i , transforming them to \mathcal{V}_i^\dagger . But since the sequence of measurements on the bath during the forward protocol was (μ_i, ν_i) , we shall take the time-reversal sequence of these outcomes, namely, (ν_i, μ_i) . As such, the corresponding time-reversed Kraus operators for the ther-

malization channels will be

$$\begin{aligned} K_{\nu_i, \mu_i}^* &:= \sqrt{\langle \nu_i | \tau_{\mathcal{B}_i} | \nu_i \rangle \langle \mu_i | \mathcal{V}_i^\dagger | \mu_i \rangle} = \sqrt{\frac{\langle \nu_i | \tau_{\mathcal{B}_i} | \nu_i \rangle}{\langle \mu_i | \tau_{\mathcal{B}_i} | \mu_i \rangle}} K_{\mu_i, \nu_i}^\dagger, \\ &= \sqrt{\frac{q_{n_{i-1}}^{(i)}}{q_{n_i}^{(i)}}} K_{\mu_i, \nu_i}^\dagger, \end{aligned} \quad (\text{A8})$$

where $q_{n_i}^{(j)} := \langle e_{n_i} | \tau_j | e_{n_i} \rangle$. Here we have used the fact that, given the energy conservation of the thermalization unitary \mathcal{V}_i , it follows that

$$\begin{aligned} \frac{\langle \nu_i | \tau_{\mathcal{B}_i} | \nu_i \rangle}{\langle \mu_i | \tau_{\mathcal{B}_i} | \mu_i \rangle} &= e^{(\epsilon_{\mu}(i) - \epsilon_{\nu}(i))/k_B T} = e^{(E_{n_i}(i) - E_{n_{i-1}}(i))/k_B T} \\ &= \frac{\langle e_{n_{i-1}} | \tau_i | e_{n_{i-1}} \rangle}{\langle e_{n_i} | \tau_i | e_{n_i} \rangle} = \frac{q_{n_{i-1}}^{(i)}}{q_{n_i}^{(i)}}, \end{aligned} \quad (\text{A9})$$

where $E_{n_i}(j) := \langle e_{n_i} | H_j | e_{n_i} \rangle$. Finally, the time-reversed trajectories can be denoted as

$$\Gamma^* = \Gamma_{(n_N, \dots, n_0, l), (\nu_1, \mu_1), (\nu_2, \mu_2), \dots, (\nu_N, \mu_N)}, \quad (\text{A10})$$

which occur with the probability

$$P^*(\Gamma^*) = \langle e_{n_N} | \tau_N | e_{n_N} \rangle \|\mathcal{K}_{\Gamma^*}\|^2, \quad (\text{A11})$$

where we introduce the time reversed Kraus operators for the full protocol,

$$\mathcal{K}_{\Gamma^*} := \sqrt{\frac{\prod_{i=1}^N q_{n_{i-1}}^{(i)}}{\prod_{i=1}^N q_{n_i}^{(i)}}} \mathcal{K}_{\Gamma}^\dagger. \quad (\text{A12})$$

Now we may evaluate the entropy production for the full protocol, which is given by Eq. (A2) and Eq. (A11) to be

$$\begin{aligned} s_{\text{irr}}(\Gamma) &:= k_B \log \frac{P(\Gamma)}{P^*(\Gamma^*)}, \\ &= k_B \log \frac{\langle \tilde{\theta}_l | \rho_{\tilde{\theta}} | \tilde{\theta}_l \rangle \|\mathcal{K}_{\Gamma}\|^2}{\langle e_{n_N} | \tau_N | e_{n_N} \rangle \|\mathcal{K}_{\Gamma^*}\|^2}, \\ &= k_B \log \frac{\langle \tilde{\theta}_l | \rho_{\tilde{\theta}} | \tilde{\theta}_l \rangle}{\langle e_{n_N} | \tau_N | e_{n_N} \rangle} + k_B \sum_{i=1}^N \log \frac{q_{n_i}^{(i)}}{q_{n_{i-1}}^{(i)}}, \end{aligned} \quad (\text{A13})$$

where we have used the fact that $\|\mathcal{K}_{\Gamma}\|^2 = \|\mathcal{K}_{\Gamma}^\dagger\|^2$. Note that the entropy production is independent of the bath measurement results. In other words, the entropy production can be purely determined by the system trajectories Γ_S .

It is trivial to show that this entropy production can be split into the three terms

$$s_{\text{irr}}(\Gamma) = s_{\text{irr}}^{\text{qu}}(\Gamma_{(l,m)}^q) + s_{\text{irr}}^{\text{cl}}(\Gamma_{(m,n)}^{\text{cl}}) + s_{\text{irr}}^{\text{cl}}(\Gamma^{(\text{IV})}), \quad (\text{A14})$$

where $s_{\text{irr}}^{\text{qu}}(\Gamma_{(l,m)}^q)$ and $s_{\text{irr}}^{\text{cl}}(\Gamma_{(m,n)}^{\text{cl}})$ are defined in Eq. (14) and Eq. (15), respectively, and

$$\begin{aligned} s_{\text{irr}}^{\text{cl}}(\Gamma^{(\text{IV})}) &:= k_B \log \frac{q_{n_1}^{(1)}}{q_{n_N}^{(N)}} + k_B \sum_{i=2}^N \log \frac{q_{n_i}^{(i)}}{q_{n_{i-1}}^{(i-1)}}, \\ &= \sum_{i=2}^N k_B \log \frac{q_{n_{i-1}}^{(i-1)}}{q_{n_{i-1}}^{(i)}} \end{aligned} \quad (\text{A15})$$

is the entropy production of Step **(IV)**.

Since the average entropy production is additive, i.e. $\langle s_{\text{irr}} \rangle_{\Gamma} = \langle s_{\text{irr}}^{\text{qu}} \rangle_{\Gamma^{\text{q}}} + \langle s_{\text{irr}}^{\text{cl}} \rangle_{\Gamma^{\text{cl}}} + \langle s_{\text{irr}}^{\text{cl}} \rangle_{\Gamma^{\text{(IV)}}$, we will compute each term separately. Let us first turn to the last term, namely, the entropy production in Step **(IV)**. We verify that averaging over the trajectory probabilities, one obtains

$$\begin{aligned} \frac{\langle s_{\text{irr}}^{\text{cl}} \rangle_{\Gamma^{\text{(IV)}}}}{k_B} &= \sum_{i=2}^N \sum_{n_{i-1}} q_{n_{i-1}}^{(i-1)} \log \frac{q_{n_{i-1}}^{(i-1)}}{q_{n_{i-1}}^{(i)}} \\ &= \sum_{i=2}^N D[\tau_{i-1} \| \tau_i]. \end{aligned} \quad (\text{A16})$$

When Step **(IV)** approaches the quasistatic limit, we will have $D[\tau_{i-1} \| \tau_i] \rightarrow 0$, and so $\langle s_{\text{irr}} \rangle_{\Gamma} = \langle s_{\text{irr}}^{\text{qu}} \rangle_{\Gamma^{\text{q}}} + \langle s_{\text{irr}}^{\text{cl}} \rangle_{\Gamma^{\text{cl}}}$.

Now we turn to the average entropy production during Step **(III)**. Using Eq. (10) and Eq. (14), and introducing the labels $p_l := \langle \tilde{\theta}_l | \rho_{\tilde{\theta}} | \tilde{\theta}_l \rangle$ and $r_m := \langle e_m | \eta_{\tilde{\theta}} | e_m \rangle$, the average quantum entropy production can be shown to be

$$\begin{aligned} \langle s_{\text{irr}}^{\text{qu}} \rangle_{\Gamma^{\text{q}}} &= \sum_{l,m} P(\Gamma_{(l,m)}^{\text{q}}) s_{\text{irr}}^{\text{qu}}(\Gamma_{(l,m)}^{\text{q}}) \\ &= k_B \sum_{l,m} p_l |\langle e_m | \tilde{\theta}_l \rangle|^2 \log \frac{p_l}{r_m} \\ &= k_B (S_{\text{vN}}(\eta_{\tilde{\theta}}) - S_{\text{vN}}(\rho_{\tilde{\theta}})) = k_B D[\rho_{\tilde{\theta}} \| \eta_{\tilde{\theta}}], \end{aligned} \quad (\text{A17})$$

as stated in the main text. Here, we used the fact that $\sum_l p_l |\langle e_m | \tilde{\theta}_l \rangle|^2 \log r_m = r_m \log r_m$, and that $\text{tr}[\eta_{\tilde{\theta}} \log \eta_{\tilde{\theta}}] = \text{tr}[\rho_{\tilde{\theta}} \log \eta_{\tilde{\theta}}]$. Meanwhile, the average classical entropy production is given by Eq. (11) and Eq. (15) as

$$\begin{aligned} \langle s_{\text{irr}}^{\text{cl}} \rangle_{\Gamma^{\text{cl}}} &= \sum_{m,n} P(\Gamma_{(m,n)}^{\text{cl}}) s_{\text{irr}}^{\text{cl}}(\Gamma_{(m,n)}^{\text{cl}}) \\ &= k_B \sum_m r_m \log \frac{r_m}{q_m} = k_B D[\eta_{\tilde{\theta}} \| \tau_1], \end{aligned} \quad (\text{A18})$$

where here $q_m := \langle e_m | \tau_1 | e_m \rangle$.

Finally, we wish to determine the fluctuations in the entropy production during Step **(III)**, quantified by the variance. The variance in the quantum entropy production can therefore be shown to be

$$\begin{aligned} \frac{\text{Var}(s_{\text{irr}}^{\text{q}})}{k_B^2} &= \sum_{l,m} \frac{P(\Gamma_{(l,m)}^{\text{q}}) s_{\text{irr}}^{\text{qu}}(\Gamma_{(l,m)}^{\text{q}})^2}{k_B^2} - D[\rho_{\tilde{\theta}} \| \eta_{\tilde{\theta}}]^2 \\ &= \sum_{l,m} p_l |\langle e_m | \tilde{\theta}_l \rangle|^2 \left(\log \frac{p_l}{r_m} \right)^2 - D[\rho_{\tilde{\theta}} \| \eta_{\tilde{\theta}}]^2 \\ &= \sum_l p_l \log^2 p_l + \sum_m r_m \log^2 r_m \\ &\quad - 2 \sum_{l,m} p_l |\langle e_m | \tilde{\theta}_l \rangle|^2 \log p_l \log r_m - D[\rho_{\tilde{\theta}} \| \eta_{\tilde{\theta}}]^2 \\ &= \text{tr}[\rho_{\tilde{\theta}} (\log^2 \rho_{\tilde{\theta}} + \log^2 \eta_{\tilde{\theta}} - 2 \log \rho_{\tilde{\theta}} \log \eta_{\tilde{\theta}})] \\ &\quad - D[\rho_{\tilde{\theta}} \| \eta_{\tilde{\theta}}]^2 \\ &= \text{tr}[\rho_{\tilde{\theta}} (\log \rho_{\tilde{\theta}} - \log \eta_{\tilde{\theta}} - D[\rho_{\tilde{\theta}} \| \eta_{\tilde{\theta}}] \mathbb{1})^2] \\ &=: \mathcal{V}[\rho_{\tilde{\theta}} \| \eta_{\tilde{\theta}}]. \end{aligned} \quad (\text{A19})$$

Here, $\mathcal{V}[\rho \| \sigma] := \text{tr}[\rho (\log \rho - \log \sigma - D[\rho \| \sigma] \mathbb{1})^2]$ is the relative entropy variance [90].

Similarly, the variance in the classical entropy production can be obtained as

$$\begin{aligned} \frac{\text{Var}(s_{\text{irr}}^{\text{cl}})}{k_B^2} &= \sum_{m,n} \frac{P(\Gamma_{(m,n)}^{\text{cl}}) s_{\text{irr}}^{\text{cl}}(\Gamma_{(m,n)}^{\text{cl}})^2}{k_B^2} - D[\eta_{\tilde{\theta}} \| \tau_1]^2 \\ &= \sum_m r_m \left(\log \frac{r_m}{q_m} \right)^2 - D[\eta_{\tilde{\theta}} \| \tau_1]^2 \\ &= \sum_m r_m \log^2 r_m + \sum_m r_m \log^2 q_m \\ &\quad - 2 \sum_m r_m \log r_m \log q_m - D[\eta_{\tilde{\theta}} \| \tau_1]^2 \\ &= \text{tr}[\eta_{\tilde{\theta}} (\log^2 \eta_{\tilde{\theta}} + \log^2 \tau_1 - 2 \log \eta_{\tilde{\theta}} \log \tau_1)] \\ &\quad - D[\eta_{\tilde{\theta}} \| \tau_1]^2 \\ &= \text{tr}[\eta_{\tilde{\theta}} (\log \eta_{\tilde{\theta}} - \log \tau_1 - D[\eta_{\tilde{\theta}} \| \tau_1] \mathbb{1})^2] \\ &=: \mathcal{V}[\eta_{\tilde{\theta}} \| \tau_1]. \end{aligned} \quad (\text{A20})$$

It is straightforward to verify that the variance in entropy production across all of Step **(III)** is $\mathcal{V}[\rho_{\tilde{\theta}} \| \tau_1]$. To see this, note that the entropy production along the full augmented trajectories $\Gamma_{(l,m,n)}^{(\text{III})}$ is given by combining Eq. (14) and Eq. (15), to obtain $k_B (\log p_l - \log q_m)$. Since the index n , corresponding to the final measurement, does not appear here, these entropy productions are associated with probabilities $P(\Gamma_{(l,m)}^{\text{q}})$. As such, the variance in entropy production is evaluated completely analogously as with Eq. (A19), and merely replacing $\eta_{\tilde{\theta}}$ and r_m with τ_1 and q_m , respectively. However, note that unlike the average entropy production, the variance in entropy production is generally not additive across the decoherence and thermalization trajectories: $\mathcal{V}[\rho_{\tilde{\theta}} \| \tau_1] \neq \mathcal{V}[\rho_{\tilde{\theta}} \| \eta_{\tilde{\theta}}] + \mathcal{V}[\eta_{\tilde{\theta}} \| \tau_1]$.

We note that, in particular, $\mathcal{V}[\eta_{\tilde{\theta}} \| \tau_1]$ has been identified as determining the efficiency of work extraction from an energy incoherent state $\eta_{\tilde{\theta}}$, with only a finite number of copies of the system [91, 92]. Namely, the work that can be ϵ -deterministically extracted per n copy of $\eta_{\tilde{\theta}}$, with small values of infidently ϵ , is given as $W = k_B T D[\eta_{\tilde{\theta}} \| \tau_1] - \Delta W$, where ΔW is a positive term that is proportional to $k_B T \sqrt{\mathcal{V}[\eta_{\tilde{\theta}} \| \tau_1] / n}$.

B. Quantum heat for a d -dimensional system

We here consider a finite d -dimensional system with Hamiltonian $H = \sum_{m=1}^d E_m |e_m\rangle \langle e_m|$ and in a state $\rho = \sum_{l=1}^d p_l |\psi_l\rangle \langle \psi_l|$. As the system decoheres with respect to the Hamiltonian, we obtain trajectories $\Gamma_{(l,m)}^{\text{q}} := |\psi_l\rangle \mapsto |e_m\rangle$, with probabilities $P(\Gamma_{(l,m)}^{\text{q}}) = p_l |\langle \psi_l | e_m \rangle|^2$ and quantum heat $Q_{\text{qu}}(\Gamma_{(l,m)}^{\text{q}}) := \langle e_m | H | e_m \rangle - \langle \psi_l | H | \psi_l \rangle$. The average quantum heat for a decoherence process is always

zero,

$$\begin{aligned}\langle Q_{\text{qu}} \rangle_{\Gamma^q} &= \sum_{l,m} P(\Gamma_{(l,m)}^q) Q_{\text{qu}}(\Gamma_{(l,m)}^q) \\ &= \sum_m \langle e_m | \rho | e_m \rangle \langle e_m | H | e_m \rangle - \text{tr}[H \rho] \\ &= 0.\end{aligned}\quad (\text{B1})$$

Hence the variance in quantum heat is equal to its second moment:

$$\begin{aligned}\text{Var}(Q_{\text{qu}}) &= \sum_{l,m} P(\Gamma_{(l,m)}^q) Q_{\text{qu}}^2(\Gamma_{(l,m)}^q) \\ &= \sum_{l,m} p_l |\langle \psi_l | e_m \rangle|^2 \langle e_m | H^2 | e_m \rangle + \sum_l p_l \langle \psi_l | H | \psi_l \rangle^2 \\ &\quad - 2 \sum_{l,m} p_l |\langle \psi_l | e_m \rangle|^2 \langle \psi_l | H | \psi_l \rangle \langle e_m | H | e_m \rangle.\end{aligned}\quad (\text{B2})$$

Noting that $\sum_m |\langle \psi_l | e_m \rangle|^2 \langle e_m | H^k | e_m \rangle = \langle \psi_l | H^k | \psi_l \rangle$, the variance reduces to

$$\begin{aligned}\text{Var}(Q_{\text{qu}}) &= \sum_l p_l (\langle \psi_l | H^2 | \psi_l \rangle - \langle \psi_l | H | \psi_l \rangle^2), \\ &= \sum_l p_l \Delta(H, \psi_l),\end{aligned}\quad (\text{B3})$$

where $\Delta(H, \rho) := \text{tr}[H^2 \rho] - \text{tr}[H \rho]^2$ is the variance of the Hamiltonian H in state ρ . In other words, the variance in quantum heat is the average variance of the Hamiltonian in the pure state components of the initial state ρ .

We now give upper and lower bounds to the variance in quantum heat for a general d -dimensional system before discussing its behaviour for the qubit case in Appendix C. For the upper bound we have

$$\begin{aligned}\Delta(H, \rho) - \text{Var}(Q_{\text{qu}}) &= \sum_l p_l \langle \psi_l | H | \psi_l \rangle^2 - \text{tr}[H \rho]^2 \\ &= \sum_l p_l (\langle \psi_l | H | \psi_l \rangle - \text{tr}[H \rho])^2 \geq 0.\end{aligned}\quad (\text{B4})$$

To obtain a lower bound, we use the fact that $\Delta(H, \rho) = I_\alpha(H, \rho)$ whenever ρ is a pure state, where $I_\alpha(H, \rho) = \text{tr}[H^2 \rho] - \text{tr}[H \rho^\alpha H \rho^{1-\alpha}]$ for $\alpha \in (0, 1)$ is the Wigner-Yanase-Dyson skew information of the observable H in ρ

[79]. Using the Lieb concavity theorem [80] it follows that

$$\text{Var}(Q_{\text{qu}}) = \sum_l p_l I_\alpha(H, \psi_l) \geq I_\alpha(H, \rho).\quad (\text{B5})$$

Combining Eq. (B4) and Eq. (B5) shows that the variance in quantum heat obeys

$$\Delta(H, \rho) \geq \text{Var}(Q_{\text{qu}}) \geq I_\alpha(H, \rho),\quad (\text{B6})$$

where the equalities are saturated only if ρ is pure.

C. Quantum and Classical heat variances for a qubit

We will now show monotonicity of $\text{Var}(Q_{\text{qu}})$ with $\text{coh}(\rho_{\tilde{\theta}})$ for the decoherence of the qubit state $\rho_{\tilde{\theta}}$ in the eigenbasis of H_1 , discussed in the main text, by explicit calculation. The quantum heat variance for the quantum decoherence trajectories $\Gamma_{(l,m)}^q$ is

$$\text{Var}(Q_{\text{qu}}) = p \Delta(H_1, \tilde{\theta}_-) + (1-p) \Delta(H_1, \tilde{\theta}_+),\quad (\text{C1})$$

where $H_1 = \frac{\hbar\omega_1}{2}(|e_+\rangle\langle e_+| - |e_-\rangle\langle e_-|)$ is the qubit Hamiltonian and the density matrix before decoherence is $\rho_{\tilde{\theta}} = p|\tilde{\theta}_-\rangle\langle\tilde{\theta}_-| + (1-p)|\tilde{\theta}_+\rangle\langle\tilde{\theta}_+|$. The Hamiltonian variance in the two eigenstates $|\tilde{\theta}_\pm\rangle$ gives the same expression,

$$\begin{aligned}\Delta(H_1, \tilde{\theta}_\pm) &= \frac{(\hbar\omega_1)^2}{4} \left(1 - [|\langle \tilde{\theta}_\pm | e_+ \rangle|^2 - |\langle \tilde{\theta}_\pm | e_- \rangle|^2]^2 \right) \\ &= (\hbar\omega_1)^2 \left[\frac{1}{4} - \left(\frac{1}{2} - \text{coh}(\rho_{\tilde{\theta}}) \right)^2 \right],\end{aligned}\quad (\text{C2})$$

where $\text{coh}(\rho_{\tilde{\theta}}) = \sin^2(\tilde{\theta}/2)$ for $\tilde{\theta} \in [-\pi/2, \pi/2]$. This shows that the quantum heat variance monotonically increases for coh ranging from 0 to 1/2.

As for the classical heat variance for the thermalization trajectories Γ^{cl} , note that there are only two trajectories which contribute non-vanishing values: $|e_-\rangle \mapsto |e_+\rangle$, with absorbed heat $\hbar\omega_1$, occurring with probability $r_{\tilde{\theta}}(1-q_1)$ with $q_1 \geq 1/2$; and $|e_+\rangle \mapsto |e_-\rangle$, with absorbed heat $-\hbar\omega_1$, occurring with probability $(1-r_{\tilde{\theta}})q_1$. Consequently, the variance is

$$\begin{aligned}\text{Var}(Q_{\text{cl}}) &= (\hbar\omega_1)^2 (r_{\tilde{\theta}}(1-q_1) + (1-r_{\tilde{\theta}})q_1) \\ &\quad - (\hbar\omega_1)^2 (r_{\tilde{\theta}} - q_1)^2 \\ &= (\hbar\omega_1)^2 (r_{\tilde{\theta}} - r_{\tilde{\theta}}^2) + (\hbar\omega_1)^2 (q_1 - q_1^2),\end{aligned}\quad (\text{C3})$$

where $r_{\tilde{\theta}} = q_1 \exp(-\text{nonth}(\rho_{\tilde{\theta}})) \geq 1/2$ is a function of the non-thermality of the state $\rho_{\tilde{\theta}}$. Hence $\text{Var}(Q_{\text{cl}})$ monotonously increases with $\text{nonth}(\rho_{\tilde{\theta}})$, see also Fig. 4.